HHS Public Access

Author manuscript

Sci Signal. Author manuscript; available in PMC 2019 December 27.

Published in final edited form as:

Sci Signal. ; 12(574): . doi:10.1126/scisignal.aau8072.

Agonist-selective NOP receptor phosphorylation correlates in vitro and in vivo and reveals differential post-activation signaling by chemically diverse agonists

Anika Mann[1,*], **Lionel Moulédous**[2], **Carine Froment**[3], **Patrick R. O´Neill**[4], **Pooja Dasgupta**[1], **Thomas Günther**[1], **Gloria Brunori**[5], **Brigitte L. Kieffer**[6], **Lawrence Toll**[5], **Michael R. Bruchas**[7], **Nurulain T. Zaveri**[8], **Stefan Schulz**[1,*]

[1]Institute of Pharmacology and Toxicology, Jena University Hospital, Friedrich Schiller University Jena, Drackendorfer Str. 1, Jena 07747, Germany.

[2]Research Center on Animal Cognition, Center for Integrative Biology, Toulouse University, CNRS, UPS, 31062 Toulouse Cedex09, France.

[3]Institut de Pharmacologie et de Biologie Structurale Université de Toulouse, CNRS, UPS, 31077 Toulouse Cedex04, France.

[4]Department of Anesthesiology, Washington University School of Medicine, St. Louis, MO 63110, USA.

[5]Biomedical Science Department, Charles E. Schmidt College of Medicine, Florida Atlantic University, Boca Raton, FL 33431, USA.

[6]Douglas Research Center, Department of Psychiatry, Faculty of Medicine, McGill University, Montreal, QC, H3A 1A1, Canada.

[7]Center for the Neurobiology of Addiction, Pain and Emotion, Departments of Anesthesiology, and Pharmacology, University of Washington, Seattle, WA 98195, USA.

[8]Astraea Therapeutics, LLC, Mountain View, CA 94043, USA.

Abstract

Agonists of the nociceptin/orphanin FQ opioid peptide (NOP) receptor, a member of the opioid receptor family, are under active investigation as novel analgesics, but their modes of signaling are less well characterized than those of other members of the opioid receptor family. Therefore, we investigated whether different NOP receptor ligands showed differential signaling or functional selectivity at the NOP receptor. Using newly developed phosphosite-specific antibodies to the

[*]Corresponding author. anika.mann@med.uni-jena.de (A.M.); Stefan.Schulz@med.uni-jena.de (S.S.).

Author contributions:

AM, SS, LM, MRB, TG, PD and PRON designed experiments. AM, TG, LM, CF, PRON, GB, PD and SS performed the experiments. AM, PD, LM, SS and PRON analyzed the data. AM wrote the manuscript. LM, NTZ, MRB, LT, BLK and SS reviewed and edited the draft. NTZ, LT, BLK and MRB provided key reagents, mouse lines and tissue samples.

Conflicts of Interest:

The authors declare that they have no conflict of interest.

Data and materials availability: The mass spectrometry proteomics data have been deposited to the ProteomeXchange Consortium (http://proteomecentral.proteomexchange.org) via the PRIDE partner repository (129) with the dataset identifier PXD012908 All other data needed to evaluate the conclusions in the paper are present in the paper or the Supplementary Materials.

NOP receptor, we found that agonist-induced NOP receptor phosphorylation occurred primarily at four carboxyl-terminal serine (Ser) and threonine (Thr) residues, namely Ser^{346}, Ser^{351}, Thr^{362}, and Ser^{363}, and proceeded with a temporal hierarchy, with Ser^{346} as the first site of phosphorylation. G protein–coupled receptor kinases 2 and 3 (GRK2/3) cooperated during agonist-induced phosphorylation, which in turn facilitated NOP receptor desensitization and internalization. A comparison of structurally distinct NOP receptor agonists revealed dissociation in functional efficacies between G protein–dependent signaling and receptor phosphorylation. Furthermore, in NOP-eGFP and NOP-eYFP mice, NOP receptor agonists induced multisite phosphorylation and internalization in a dose-dependent and agonist-selective manner that could be blocked by specific antagonists. Our study provides new tools to study ligand-activated NOP receptor signaling in vitro and in vivo. Differential agonist-selective NOP receptor phosphorylation by chemically diverse NOP receptor agonists suggests that differential signaling by NOP receptor agonists may play a role in NOP receptor ligand pharmacology.

Introduction

The nociceptin/orphanin FQ peptide receptor (NOP receptor; NOPR) is the fourth-discovered member of the opioid receptor family and is still the least characterized member (1–4). An endogenous neuropeptide identified from rat and porcine brain extracts was found to activate the NOP receptor by inhibiting cyclic adenosine monophosphate (cAMP) accumulation in transfected cells and was named nociceptin/orphanin FQ (N/OFQ) (5, 6). Through coupling to $G\alpha_i/G\alpha_0$ proteins, NOP receptor activation by N/OFQ leads to inhibition of adenylate cyclase and calcium channels (N-, L- and P/Q-type), as well as the activation of G protein-coupled inwardly rectifying potassium (GIRK) channels (3, 6–14). In addition, various proteins such as protein kinase C (PKC), phospholipase A2 (PLA2), extracellular signal-regulated kinase 1 (ERK1) and ERK2, p38 mitogen-activated protein kinase (MAPK) and c-Jun N-terminal kinase (JNK) are also activated by NOP receptors (12, 15–20). The NOP receptor is widely expressed throughout the brain, spinal cord and dorsal root ganglia (DRG) (21–26) and is involved in the regulation of important physiological processes, such as learning and memory, emotion, food intake, locomotion, respiration, and immune defense (6, 27–35). NOP receptors are also involved in renal, cardiovascular and gastrointestinal functions, as well as pain perception, addiction and tolerance development (36–41).

The NOP receptor is under active investigation as a therapeutic drug target for many indications. Non-peptidic, small-molecule NOP receptor agonists have been investigated preclinically as anxiolytics and substance abuse medications, and clinically as potential anti-tussives (42). Being in the opioid receptor family, the NOP receptor has been shown to modulate the classical mu opioid (MOP) receptor pharmacology in pain and reward pathways. Intracerebroventricular N/OFQ administration can block morphine, cocaine, alcohol, or methamphetamine induced rewarding effects, as well as increases in extracellular dopamine in mesolimbic pathways (43–48). Novel analgesics with bifunctional activity targeting the MOP and NOP receptor have been developed, one of which is in clinical trials. (49–61). Cebranopadol, the first bifunctional MOP/NOP receptor agonist to reach Phase III clinical trials for acute and chronic pain, has potent anti-nociceptive activity in rodent pain

models and is ~1000 times more potent and longer-lasting than morphine in chronic pain assays (59, 61). Cebranopadol exhibited a reduced side-effect profile including development of tolerance, motor deficits or respiratory depression compared with classical MOP receptor agonists (58, 60–65). AT-121, a MOP/NOP receptor bifunctional ligand with partial agonist activity at both receptors, was reported to show morphine-comparable analgesic effects in nonhuman primates, and no side effects such as respiratory depression, abuse potential and physical dependence (66).

Given the global opioid epidemic, alternatives and approaches to decrease the side-effects of classical opioid-based drugs have focused on biased ligands which preferentially activate the G protein-dependent signaling cascades over the G protein-independent signaling, such as arrestin-mediated signaling (67–70). Such differential activation was found to lead to a dissociation of analgesic effects from adverse effects such as respiratory depression, gastrointestinal effects and tolerance, the former considered a G protein-mediated effect (analgesic efficacy) and the latter (undesired effects) due to arrestin recruitment. Such correlations form the fundamental basis for the development of the biased MOP receptor agonist TRV130 that recently completed Phase III clinical (70–75). TRV130 is “biased” for the G protein-mediated pathway over the arrestin pathway, and shows markedly reduced receptor internalization and arrestin recruitment (76, 77).

The clinical use of drugs targeting NOP receptors requires a profound understanding of the NOP receptor system at the physiological and molecular levels. However, much less is understood about NOP receptor signaling after ligand binding. A report by Chang *et al.* (78) showed that various NOP receptor agonists had differential efficacy in activating G-protein-dependent cAMP inhibition compared to G protein-independent arrestin recruitment, leading to functional selectivity or “signaling bias”. Similarly, other studies demonstrated that NOP receptor partial agonist AT-090 showed arrestin-biased functional selectivity in recombinant cells (79). The detailed molecular events occurring after ligand binding that lead to signaling bias at the NOP receptor are not as yet completely unraveled. In particular, key events in the regulation of GPCRs such as receptor phosphorylation, internalization and desensitization that have been characterized in great detail for the classical opioid GPCRs are not well understood for the NOP receptor (80–86). For example, in the closely-related MOP receptor, a cluster of four carboxyl-terminal serine (Ser) and threonine (Thr) residues, namely Ser^{375}, Thr^{370}, Thr^{376} and Thr^{379} are phosphorylated by GPCR kinases 2 and 3 (GRK2/3) as well as GRK5 in an agonist-selective and hierarchical manner (87–89). Our own studies with MOP receptor show that its phosphorylation and internalization occurs in an agonist-specific and time-dependent manner and is determined by a 10-residue sequence in the carboxyl-terminal tail of the receptor. Ser^{375}, present in the middle of this sequence, is phosphorylated by many opioids. Morphine, oxycodone and buprenorphine stimulate phosphorylation only at Ser^{375} and the morphine-induced phosphorylation is mediated by GRK5 (88–90). But there are marked differences in driving higher-order phosphorylation on flanking residues (Thr^{370}, Thr^{376} and Thr^{379}) between opioids. Multisite-phosphorylation induced by fentanyl, DAMGO, and etorphine requires GRK2/3 (88, 89). Also opioid induced receptor internalization is controlled by higher-order phosphorylation involving Thr^{370}, Thr^{376} and Thr^{379} (89).

In case of the NOP receptor, it is known that GRK2 and GRK3 are relevant for NOP receptor desensitization (91–93). Additionally, GRK3 and ß-arrestin2 appear to be important for N/OFQ-induced internalization, because point mutation of Ser^{363} reduces, but not completely blocks, NOP receptor internalization (12). It is possible that several phosphorylation sites are essential for internalization and desensitization of the NOP receptor. Further, given the differential functional selectivity amongst chemically diverse reported NOP receptor agonists, it is possible that different agonists may induce recruitment of one or more GRK isoforms to the NOP receptor. Here, we investigated the mechanisms of agonist-induced NOP receptor phosphorylation by generating and extensively characterizing the first phosphosite-specific antibodies for the NOP receptor carboxyl-terminal residues Ser^{346}, Ser^{351} and Thr^{362}/Ser^{363}. These allowed us to selectively detect multiple phosphorylated forms of NOP receptor in vitro and in vivo after treatment with chemically diverse NOP receptor agonists.

Results

Phosphosite-specific antibodies reveal spatial and temporal dynamics of agonist-induced phosphorylation of Ser^{346}, Ser^{351} and Thr^{362}/Ser^{363} in the carboxyl-terminal tail of the NOP receptor.

The human NOP receptor contains a number of potential phosphate acceptor sites in its intracellular loops as well as within its carboxyl-terminal tail (Fig. 1A). In whole-cell phosphorylation assays, we observed a robust increase in NOP receptor phosphorylation after addition of its endogenous ligand N/OFQ (Fig. 1B). Notably, this increase was not observed in a NOP receptor mutant (6S/T-A) in which all six carboxyl-terminal serine and threonine residues were exchanged to alanine (Fig. 1B). This finding suggests that agonist-induced NOP receptor phosphorylation occurs primarily within its carboxyl-terminal tail. In an effort to examine the temporal and spatial dynamics of NOP receptor phosphorylation, we generated polyclonal phosphosite-specific antibodies for the carboxyl-terminal residues Ser^{346}, Ser^{351} and Thr^{362}/Ser^{363} (Fig. 1A). In addition, we also generated a polyclonal phosphorylation-independent antibody to the NOP receptor (NOPR) (Fig. 1A). First, antisera were affinity purified against their immunizing peptides and specificity was then verified with synthetic phosphopeptides and corresponding nonphosphopeptides using dot-blot assays (Fig. 1C). All antibodies, which clearly detected their respective peptide without cross-reaction with the nonphosphopeptide, were further characterized using Western blot analysis. The anti-$pSer^{346}$ antibody, anti-$pSer^{351}$ antibody and anti-Thr^{362}/Ser^{363} antibody specifically detected the respective Ser^{346}-, Ser^{351}- or Thr^{362}/Ser^{363}-phosphorylated form of the NOP receptor after N/OFQ incubation of human embryonic kidney (HEK) 293 cells stably transfected with the human NOP receptor (Fig. 1, D and E). After treatment with lambda phosphatase, all phosphosite-specific antibodies were no longer able to detect their cognate forms of phosphorylated NOP receptors, whereas the receptor protein was still detectable using the phosphorylation-independent NOPR antibody (Fig. 1, D and E).

For further characterization of the phosphosite-specific antibodies, different NOP receptor mutants were generated (Fig. 2A). Immunoblot analysis showed that N/OFQ strongly stimulated phosphorylation at Ser^{346}, Ser^{351} and Thr^{362}/Ser^{363}. As expected, receptor

phosphorylation was not detectable after global mutation of all serine and threonine residues present in the carboxyl-terminal tail (6S/T-A) or in a mutant with additional mutation of all serine and threonine residues within the third intracellular loop (10S/T-A). No phosphorylation signal for pSer^{346} and pSer^{351} was detectable in the S337A/S346A/S351A mutant (Fig. 2, B and C, left columns). Conversely, receptor constructs with a T362A/S363A/T365A mutation and an S363A point mutation displayed no binding of the anti-pThr^{362}/pSer^{363} antibody after N/OFQ stimulation (Fig. 2B, middle column). It should be noted that the phosphorylation-independent NOPR antibody was not able to detect any protein band corresponding to the mutant construct T362A/S363A/T365A, suggesting that this sequence may contribute to the epitope recognized by the antibody (Fig. 2B, right column). Probing for the HA-epitope tag ensured that the T362A/S363A/T365A construct was indeed expressed, as well as all other NOP receptor constructs used in this study (Fig. 2, B and C, bottom row). These results confirm that we generated phosphosite-specific antibodies directed against Ser^{346}, Ser^{351} and Thr^{362}/Ser^{363} in the carboxyl-terminal tail.

NOP receptor phosphorylation occurs in a time-dependent manner with Ser^{346} as primary phosphorylation site followed by Ser^{351} and Thr^{362}/Ser^{363}.

We then examined the time-course of N/OFQ-induced Ser^{346}, Ser^{351} and Thr^{362}/Ser^{363} phosphorylation and receptor internalization in vitro. After N/OFQ treatment, a robust phosphorylation at Ser^{346} and Ser^{351} was detectable within 1 min, and remained abundant throughout the 60 min treatment period, whereas Thr^{362}/Ser^{363} phosphorylation was first detectable after 1 min after the addition of N/OFQ and increased steadily throughout the 60 min treatment period (Fig. 3, A and B). To resolve the phosphorylation time-course in more detail, cells were exposed to N/OFQ at room temperature (RT) for shorter time periods. Under these conditions, S346 phosphorylation occurred within 20 s and Ser^{351} phosphorylation within 60 s, whereas Thr^{362}/Ser^{363} phosphorylation became first detectable after 3 min, suggesting that Ser^{346} is the primary site of phosphorylation, followed by Ser^{351} and Thr^{362}/Ser^{363} (Fig. 3, C and D).

The time-course of NOP receptor internalization was visualized by fluorescence microscopy and quantified using a cell-surface enzyme-linked immunosorbent assay (ELISA). NOP receptor internalization was first detectable after 5 min and reached a maximum after 60 min of agonist treatment (Fig. 3, E and F). These data indicate that N/OFQ-induced NOP receptor phosphorylation and internalization occur in a time-dependent manner with Ser^{346} as primary phosphorylation site followed by Ser^{351} and Thr^{362}/Ser^{363}.

NOP receptor phosphorylation is mediated by GRK2 and GRK3.

Phosphorylation of GPCRs can be mediated by GPCR kinases (GRKs) or second messenger-activated kinases (such as PKA and PKC). We therefore incubated cells with phorbol 12-myristate 13-acetate (PMA) or forskolin and examined NOP receptor phosphorylation. Forskolin, which activates adenylyl cyclase (and consequently cAMP-dependent protein kinases), did not produce any detectable phosphorylation of Ser^{346}, Ser^{351} or Thr^{362}/Ser^{363}. However, activation of PKC by PMA induced selective phosphorylation of Ser^{346} and Ser^{351}, indicating that Ser^{346} and Ser^{351} can also undergo heterologous PKC-mediated phosphorylation (Fig. 4A). To evaluate the contributions of GRKs to agonist-

induced NOP receptor phosphorylation, we used chemical inhibitors as well as siRNA knockdown of GRK2/3. In fact, inhibition of GRK2/3 using the selective inhibitor compound 101 reduced N/OFQ-induced phosphorylation at Ser^{346}, Ser^{351} and Thr^{362}/Ser^{363} in a concentration-dependent manner (Fig 4, A and B). Treatment with specific GRK2 or GRK3 siRNA sequences also led to a significant reduction of N/OFQ-induced phosphorylation of these residues (Fig. 4C, fig. S1A). Given the close relationship between GRK2 and GRK3, it is possible that the loss of one isoform could be compensated for by the other isoform. Therefore, we evaluated the inhibitory effect of siRNA knockdown of both GRK2 and GRK3. Indeed, combined siRNA knockdown of both GRK isoforms produced a stronger inhibition of Ser^{346}, Ser^{351} and Thr^{362}/Ser^{363} phosphorylation, indicating that GRK2 and GRK3 function as a redundant system for agonist-induced NOP receptor phosphorylation (Fig. 4C, fig. S2A). To confirm these results, we performed GRK2 and GRK3 plasmid overexpression experiments. As expected, overexpression of GRK2 or GRK3 strongly enhanced N/OFQ-induced Ser^{346}, Ser^{351} and Thr^{362}/Ser^{363} phosphorylation (Fig. 4D, fig. S1B). These results suggest that GRK2 and GRK3 are responsible for N/OFQ-induced NOP receptor phosphorylation.

Chemically diverse small-molecule NOP receptor agonists induce varying amounts of NOP receptor phosphorylation and internalization.

We next examined a range of chemically diverse NOP receptor ligands for their ability to induce NOP receptor phosphorylation and internalization. We consistently observed that the endocytotic activity of these agonists was associated with their ability to induce receptor phosphorylation at Ser^{346}, Ser^{351} and Thr^{362}/Ser^{363} (Fig. 5, A to D, and fig. S2). As expected, other endogenous or clinically-relevant opioids did not induce any detectable phosphorylation of these residues (fig. S3). Notably, our results reveal a correlation between G protein signaling and receptor phosphorylation, with NNC 63–0532 as an exception. Although MCOPPB, Ro64–6198, SCH221510, AT-202 and NNC 63–0532 strongly activated G protein signaling, only MCOPPB, Ro64–6198, SCH221510 and AT-202, but not NNC 63–0532, were able to induce robust multisite phosphorylation of the NOP receptor. Cebranopadol was also not capable of inducing either phosphorylation or NOP receptor internalization. To investigate the relationship between ligand-induced NOP receptor phosphorylation and internalization, phosphorylation values and internalization values were compared from every compound at a concentration of 10 μM (Fig. 5E and fig. S2). A direct positive linear correlation ($r = 0.8581$) was observed between the phosphorylation at Thr^{362}/Ser^{363} and receptor internalization (Ser^{346}: $r = 0.8260$ and Ser^{351}: $r = 0.7877$), indicating a relationship between the two events.

These results show that the NOP receptor phosphorylation and internalization is agonist-selective and may indicate biased coupling to intracellular signaling pathways in NOP receptors activated by NNC 63–0532.

Chemically diverse NOP receptor agonists show varying levels of functional efficacies in GIRK channel activation (G protein-dependent signaling).

To analyze G protein signaling of NOP receptor at high temporal resolution, we used a previously described fluorescence-based membrane potential assay that detects Gβγ-

dependent activation of inwardly rectifying potassium (GIRK) channels (94). AtT-20 cells, a mouse pituitary tumor cell line, stably transfected with NOP receptor were loaded with membrane potential dye. Addition of N/OFQ induced a dose-dependent decrease in fluorescence intensity, which is indicative of membrane hyperpolarization (fig. S4, A and B). Half-maximal effective concentration (EC_{50}) for N/OFQ was 1.5 ± 0.4 nM. Overnight treatment with pertussis toxin (PTX) inhibited the N/OFQ-induced hyperpolarization (fig. S4C). Addition of SCH23390, a potent and selective GIRK channel blocker, reversed the N/OFQ-evoked hyperpolarization (fig. S4D). Collectively, these results indicate that NOP receptors can couple to GIRK channels endogenously expressed in AtT-20 cells. Next, we evaluated the ability of a variety of NOP receptor ligands to activate GIRK channels (Fig. 6, A to G). Notably, MCOPPB was the most potent agonist tested with an EC_{50} of 0.06 ± 0.02 nM compared to N/OFQ (EC_{50} of 1.5 ± 0.4 nM) (Fig. 6B). SCH221510 and Ro64–6198 exhibited similar dose-response curves with EC_{50} values of 14.4 ± 3.2 nM and 15.9 ± 3.5 nM, respectively (Fig. 6, A and C). NNC 63–0532 and AT-202 (SR16835) are similar potent agonists with EC_{50} values of 56.0 ± 9.3 nM and 29.2 ± 4.7 nM, respectively (Fig. 6, D and E). Buprenorphine and cebranopadol exhibited partial agonistic activity with a remarkably reduced maximal effect compared with N/OFQ (Fig. 6, F and G). Correlation analysis were done to investigate the relationship between ligand-induced NOP receptor phosphorylation and GIRK channel activation, phosphorylation values and E_{max} values from the GIRK channel activation assay were used from every ligand (Fig. 6H). A direct positive linear correlation with a correlation coefficient of r = 0.68659 was observed between the phosphorylation at Thr^{362}/Ser^{363} and GIRK channel activation. These results show that NOP receptor mediated G protein signaling is agonist-dependent and that there exists a direct correlation between phosphorylation and GIRK channel activation.

NOP receptor antagonists selectively inhibit N/OFQ-induced phosphorylation and internalization in vitro.

The opioid receptor antagonist naloxone did not inhibit NOP receptor phosphorylation or internalization after N/OFQ treatment (Fig. 7, A to D). In contrast, the selective NOP receptor antagonists J-113397 and SB 612111 (95, 96) completely blocked N/OFQ-induced phosphorylation at Ser^{346}, Ser^{351} and Thr^{362}/Ser^{363} (Fig. 7, A and B). J-113397, but not naloxone, was also able to block N/OFQ-induced internalization (Fig. 7, C and D). Only selective NOP receptor antagonists could inhibit N/OFQ-induced phosphorylation and internalization.

NOP receptor phosphorylation is also observed in vivo after systemic treatment with NOP receptor agonists.

Using the phosphosite-specific antibodies, we analyzed NOP receptor tissue distribution using Western blot. We were able to detect the NOP receptor in the brain, spinal cord and dorsal root ganglia (DRG), but not in the lung, heart, bladder, kidney and adrenal gland (Fig. 8A). For in vivo analysis of NOP receptor phosphorylation, the non-peptide full agonist AT-202 was administered by intraperitoneal (i.p.) injection to three mice. This NOP receptor agonist allows for systemic administration with significant central bioavailability (50, 54, 97). Several peptides from the third transmembrane helix and the C-terminal part of the mouse NOP receptor were identified by nanoLC-MS/MS under basal conditions and after in

vivo AT-202 treatment. In particular, phosphorylation of Ser^{343} (equivalent to human Ser^{346}) and Thr^{359}/Ser^{360} (equivalent to human Thr^{362}/Ser^{363}) in the carboxyl-terminal tail (black symbols) could be demonstrated by CID/ETD fragmentation analysis (Fig. 8, B and C). The ^{339}EMQVSDRVR^{347} peptide containing Ser^{343} was found only in its phosphorylated form in both saline and AT-202-treated samples (Fig. 8D). On the contrary, the ^{359}TSETVPRPAGSIATMVSK^{376} peptide was detected in its Thr^{359} or Ser^{360} monophosphorylated form only in AT-202 samples (Fig. 8E) whereas the unphosphorylated peptide was present under both conditions. The lack of Thr^{359}/Ser^{360} diphosphorylated peptide suggests that only phosphorylation of either Thr^{359} or Ser^{360} is induced by AT-202. These data indicate that NOP receptor is expressed in the mouse central nervous system and that Ser^{343} and Thr^{359}/Ser^{360} are important phosphorylation sites in vivo after agonist treatment.

Agonist-selective NOP receptor phosphorylation and internalization in mouse brain.

To analyze in more detail the agonist-induced NOP receptor phosphorylation in vivo, NOP-eGFP mice were treated with different types of NOP receptor ligands. The corresponding mouse NOP receptor phosphorylation sites are located at equivalent positions compared to the human NOP receptor (Fig 9A). This fact enables us to use the phosphorylation-dependent antibodies directed against human residues to detect agonist-induced phosphorylation at mouse residues Ser^{343} (equivalent in human Ser^{346}), Ser^{348} (equivalent in human Ser^{351}) and Thr^{359}/Ser^{360} (equivalent in human Thr^{362}/Ser^{363}). To analyze NOP receptor internalization in vivo, ventral midbrain neurons from NOPR-eYFP mice were used. The MS data as well as the in vivo Western blot phosphorylation data show that there is a constitutive phosphorylation of Ser^{346} and Ser^{351} in mouse brain. The AT-202-induced phosphorylation signal occurs in a concentration-dependent manner (Fig. 9B, fig. S5A) and could be blocked by the NOP receptor-selective antagonist SB 612111 (Fig. 9C, fig. S5B). To evaluate the in vivo contribution of GRKs to AT-202-induced NOP receptor phosphorylation, we used the selective GRK2/3 inhibitor compound 101. In fact, inhibition of GRK2/3 using compound 101 blocked the AT-202-induced phosphorylation at Thr^{362}/Ser^{363} in a concentration-dependent manner (Fig. 9D). These results suggest that GRK2 and GRK3 are also responsible for AT-202-induced NOP receptor phosphorylation in vivo. AT-202, Ro64–6198 and SCH221510, but not NNC 63–0532, induced strong NOP receptor phosphorylation at Ser^{343} (equivalent in human Ser^{346}), Ser^{348} (equivalent in human Ser^{351}) and Thr^{359}/Ser^{360} (equivalent in human Thr^{362}/Ser^{363}), as well as receptor internalization (Fig. 9, E to G, fig. S5C). Only a weak escalation of phosphorylation signal was detectable after administration of NOP receptor agonist MCOPPB in comparison to the treatment with saline at Ser^{348} (equivalent in human S351) and Thr^{359}/Ser^{360} (equivalent in human Thr^{362}/Ser^{363}) (Fig. 9E, fig. S5C). In contrast, there was a strong MCOPPB-induced NOP receptor internalization and phosphorylation signal at Ser^{343} (equivalent in human Ser^{346}) detectable (Fig. 9, E to G, fig. S5C). Moreover, addition of NOP receptor antagonist J-113397 blocked the N/OFQ-induced internalization (Fig. 9, F and G). These results indicate that the NOP receptor phosphorylation and internalization occurs in an agonist-selective manner.

Discussion

Using the first phosphosite-specific antibodies for the NOP receptor, we found evidence for hierarchical and temporally controlled multisite-phosphorylation of NOP receptors, both in vitro and in vivo. Moreover, we detected distinctive ligand-selective phosphorylation patterns. The canonical model for GPCR activation/deactivation cycle postulates the following steps: The agonist-bound receptor/G protein complex becomes a substrate for GRKs or second messenger-dependent protein kinases. Phosphorylation by GRKs increases the affinity for β-arrestins, which uncouple the receptor from its G protein and target it to clathrin-coated pits for internalization, thus desensitizing the primary signaling while simultaneously initiating β-arrestin-dependent signaling. Internalized GPCRs are either trafficked to lysosomes for degradation or recycle back through an endosomal pathway.

Agonist-induced phosphorylation has been studied in great detail for several GPCRs, most notably β2-adrenoceptor (β2-AR), MOP receptor, somatostatin sst2, sst3 and sst5 receptor subtypes, and angiotensin II AT1a receptors (87–89, 98–110). The emerging picture obtained from these studies suggests that the endogenous agonist N/OFQ induces phosphorylation that proceeds in a temporal hierarchy, involving multiple serine and threonine residues located in the carboxyl-terminal domain of the NOP receptor. In each GPCR case, a primary phosphate-acceptor site has been identified and phosphorylation levels positively correlate with receptor internalization levels. In contrast, many synthetic agonists were found to produce only partial receptor phosphorylation, combined with reduced agonist-stimulated internalization. These observations support the general hypothesis that exhaustive GPCR phosphorylation is a prerequisite for internalization and a hallmark of full agonists.

For human NOP receptors, we identified Ser^{346} as the primary phosphorylation site and hierarchical phosphorylation continued thereafter to include Ser^{351}, Thr^{362} and Ser^{363}. Stimulation with N/OFQ induced maximal receptor internalization, although with slower kinetics than the closely related MOP receptor (88, 106). Thr^{362}/Ser^{363} in the NOP receptor are phosphorylated by GRK2/3-mediated phosphorylation in vitro. In contrast, Ser^{346} and Ser^{351} are also substrates for heterologous PKC phosphorylation. In MOP receptor also two phosphorylation sites (Thr^{370} and Ser^{363}) are phosphorylated by PKC (106). In vivo, AT-202-induced Thr^{362}/Ser^{363} phosphorylation is also predominantly mediated by GRK2/3. Nevertheless, a function of GRK5/6 in NOP receptor regulation and signaling cannot be ruled out.

Similar to MOP receptor agonists (88–90), most synthetic NOP receptor agonists displayed reduced potencies to stimulate receptor phosphorylation, which appeared to correlate with the level of agonist-induced internalization. One notable exception is MCOPPB, which has been described as 10-fold more potent than N/OFQ in inhibiting cAMP accumulation and displaying strong G protein-biased signaling (78, 111). Our results from GIRK channel activation assay support these previous findings. MCOPPB was also the only synthetic agonist that exhibited similar potency as N/OFQ to induce NOP receptor phosphorylation in vitro. NOP receptor agonists SCH221510 and Ro64–6198 have been previously described as full agonists in G protein-dependent cAMP assay (55, 78). We confirmed these results with

our study. Agonist AT-202 was described as a modestly selective NOP receptor full agonist, with very low efficacy at MOP receptor (54). In our GIRK channel activation assay, we confirmed that AT-202 acted as a NOP receptor full agonist. In contrast, the small-molecule NOP receptor agonist NNC 63–0532 failed to induce any phosphorylation at the NOP receptor, but behaved as a full agonist in G protein-mediated GIRK channel activation, albeit with about 40-fold reduced potency compared to N/OFQ. The opioid agonist buprenorphine, which also shows low agonist efficacy at NOP receptor (67, 112–116), displayed partial agonism in G protein-mediated GIRK assay. NNC 63–0532 and buprenorphine had previously been described as partial agonists at the NOP receptor in cAMP inhibition assays (78). Notably, the same study revealed an almost complete absence of β-arrestin recruitment, which is consistent with the complete lack of NOP receptor phosphorylation by both agonists. Morphine and fentanyl are the most effective drugs for the treatment of severe pain. But severe side effects, misuse of opioids and opioid addiction limit their use in clinical setting so that the development of addiction-free effective opioids for treating severe pain is required. Cebranopadol is the first bifunctional MOP/NOP receptor agonist that is in advanced clinical trials for the treatment of acute and chronic pain (58, 59) and has previously been described as full agonist in calcium mobilization and BRET studies (63) as well as in GTPγS assays (59). In our phosphorylation studies as well as the GIRK channel activation assay, cebranopadol clearly behaved as partial agonist at the NOP receptor. AT-121 is another bifunctional partial agonist at MOP/NOP receptor that is able to suppress oxycodone-induced reinforcing effects and elicit morphine-like analgesic effect without common side effects of classical opiods (66). Full NOP receptor agonists such as Ro64–6198 or AT-202 often induce a strong decrease in locomotor activity in vivo which limits their clinical utility (50, 117). Both cebranopadol and AT-121 are devoid of this activity suggesting that partial agonism may be a desired property for the development of bifunctional MOP/NOP receptor ligands as effective painkillers with fewer side effects.

Localization of NOP receptor has been characterized using in vitro autoradiography, in situ hybridization and immunofluorescence staining (1–3, 22–26, 118–121). Most notably, we could detect NOP receptor in the brain, spinal cord and dorsal root ganglia. from untreated mice by mass spectrometry and Western blotting. Studies have used the same techniques to analyze phosphorylation at MOP receptors (88, 103, 106, 122). In case of NOP receptor, Ser^{346}, Thr^{359} and Ser^{360}, were uncovered in the brain after AT-202 administration, whereas Ser^{343} and Ser^{348} are constitutively phosphorylated in the absence of agonist. This basal phosphorylation may reflect high constitutive activity of the NOP receptor. Nevertheless, after agonist injection, an increase of phosphorylation at both these sites was also observed. AT-202-induced phosphorylation occurred in a dose-dependent manner and could be blocked with SB 612111. In accordance with the corresponding human phosphorylation sites, in vivo phosphorylation in mice occurred in an agonist-selective manner, similarly to the MOP receptor (103). MCOPPB administration enhanced NOP receptor phosphorylation only at Ser^{343} and Thr^{359}/Ser^{360} but not Ser^{348}. In MOP receptor, in vivo, morphine induced phosphorylation only at Ser^{375} (103). NOP receptor internalization in vivo occurred also in an agonist-dependent manner and could be blocked by J-113397.

In conclusion, we identified an agonist-selective phosphorylation pattern in the carboxyl-terminal domain of the NOP receptor in vitro and in vivo that correlates with receptor

internalization. It is conceivable that the selective phosphorylation patterns provide an indication of a general biochemical mechanism by which the different functional effects of N/OFQ might be explained. Further, differential phosphorylation patterns amongst non-peptidic NOP receptor agonists suggests that structure-function correlations may be possible for the NOP receptor and may explain the differences in NOP receptor agonist pharmacology. This study provides important tools to characterize agonist-dependent regulation of NOP receptor signaling at the cellular level, which may be beneficial for the development and characterization of NOP receptor agonists for therapeutic indications.

Materials and Methods

Animals

NOP-eGFP mice (8–12 weeks old) were used to detect NOP receptor phosphorylation in vivo. Animals were group-housed under standard laboratory conditions and kept on a 12 hours day/night cycle (lights on at 7:00 A.M.) at constant temperature (20–22 °C) and humidity (45–55 °C) with *ad libitum* access to food and water. Animals were handled three times before the experiment. Mice were maintained in accordance with the National Institutes of Health (NIH) *Guide for the Care and Use of Laboratory Animals* and the Thuringian state authorities and complied with *European Commission regulations for the care and use of laboratory animals*. All methods used were preapproved by the Institutional Animal Care and Use Committee at the Torrey Pines Institute for Molecular Studies (Port St Lucie) and the University Hospital Jena, Institute of Pharmacology and Toxicology (Jena).

NOPR-eYFP mice were used to detect NOP receptor internalization in primary neurons. For these mice, eYFP was knocked into exon 4 of NOP receptor and fused at the C-terminus of the receptor, flanked on both sides by loxP sites. Embryonic mice were removed from euthanized pregnant female mice on gestational day 14 (E14) and used for ventral midbrain dissection. All procedures were approved by the Animal Care and Use Committee of Washington University and adhered to NIH guidelines.

Plasmids

DNA for human NOP receptor and human NOP receptor mutants were generated via artificial synthesis and cloned into pcDNA3.1 by imaGenes and Eurofins, respectively. The coding sequence for an amino-terminal HA-tag was added. Human GRK2 and GRK3 plasmids were obtained from OriGene and TransOMIC, respectively.

Antibodies

Peptide sequences used for generating phosphosite-specific antibodies against individual phosphorylated forms of the NOP receptor are shown in Table 1, including a phosphorylation-independent antiserum targeting a distal epitope in the NOP receptor carboxyl-terminal domain. The respective peptides were coupled to keyhole limpet haemocyanin after HPLC purification. The conjugates were mixed 1:1 with Freundś adjuvant and injected into groups of two or three rabbits (5033, 5034) for anti-pSer^{346} antibody production, (4876, 4878) for anti-pSer^{351} antibody production, (4873–4875) for anti-pThr^{362}/Ser^{363} antibody production, and (4870–4872) for anti-NOP receptor antibody

production. The rabbits were injected at 4-week intervals and serum was obtained 2 weeks after immunizations, beginning with the second injection. Using dot blot analysis, specificity of the antisera was tested. For subsequent analysis, antibodies were affinity-purified against their immunizing peptide, immobilized using the SulfoLink kit (Thermo Scientific). Generation and characterization of the polyclonal rabbit anti-HA antibody was previously described (123). Anti-GRK2 (sc-562), anti-GRK3 (sc-563) and anti-rabbit IgG HRP-coupled (sc-2004) antibodies were obtained from Santa Cruz Biotechnology. The anti-HA IgG CF™488A antibody (SAB4600054) was purchased from Sigma-Aldrich. Anti-rabbit Alexa488-coupled antibody (A11008) was obtained from Invitrogen.

Drugs

The NOP receptor agonist AT-202 was synthesized and provided by Astraea Therapeutics. Ro64–6198 was provided by Roche. Nociceptin (ab120070) and dynorphin A (ab120412) were obtained from Abcam. MCOPPB (PZ0159), ß-endorphin (E6261), DADLE (E7131), DAMGO (E7384), etonitazene (E5007), etorphine, fentanyl (F3886), hydromorphone (H5136), [Met]-enkephalin (M6638), morphine-6-glucuronide (M3528), oxycodone (O1378), pentazocine (P134), tapentadol (T058), naloxone (N7758) and PMA (P8139) were purchased from Sigma-Aldrich. SCH221510 (3240), NNC 63–0532 (1780), J-113397 (2598), SB 612111 (3573), DPDPE (1431), endomorphin-1 (1055), endomorphin-2 (1056), U50488 (0495), PTX (3097), SCH23390 (0925) and forskolin (1099) were obtained from Tocris. Norbuprenorphine (BUP-982-FB) and buprenorphine (BUP-399-HC) were purchased from Lipomed. γ-Endorphin (60893–02-9) was obtained from Bachem and tramadol from Grunenthal. Levomethadone (00424906) and pethidine (03012446) were purchased from Sanofi-Aventis. Morphine (26–6) was obtained from Merck Pharma. Nalfurafine (A12579) was purchased from Adooqioscience LLC. Piritramid and sufentanil were obtained from Hameln Pharma Plus. Remifentanil was purchased from GlaxoSmithKline. Nortilidine was obtained from Pfizer AG. Cebranopadol (HY-15536) was purchased from MedChem Express. Lambda-phosphatase (P0753S) was obtained from Santa Cruz. Compound 101 (HB2840) was obtained from Hello Bio. Tertiapin-Q was purchased from Alomone Labs. AT-202, Ro64–6198, PMA, SCH221510, NNC 63–0532, J-11339, SB 612111, DPDPE, U50488, forskolin, nalfurafine and cebranopadol are DMSO-soluble and all the other mentioned compounds are water-soluble.

Cell culture and transfection

Human embryonic kidney 293 (HEK293) cells were obtained from the German Collection of Microorganisms and Cell Cultures GmbH (Deutsche Sammlung von Mikroorganismen und Zellkulturen; DSMZ). AtT20-D16v-F2 (AtT20) cells were purchased from American Type Tissue Culture Collection. All cells were cultured at 37 °C and 5% CO_2 in Dulbeccós modified Eaglés medium (DMEM), supplemented with 10% fetal bovine serum, 2 mM L-glutamine and 100 U/ml penicillin/streptomycin. HEK293 cells and AtT20 cells were stably transfected with TurboFect (ThermoFisher Scientific). Stable transfected cells were selected in medium supplemented with 400 μg/ml geneticin.

Fluorescence-activated cell sorting (FACS)

To increase the number of HEK293 cells or AtT20 cells stably expressing the hNOP receptor or mutant hNOP receptors, FACS was used. Cells were incubated with trypsin, washed with PBS, resuspended in OPTI-MEM containing anti-HA IgG, CF™488 antibody (Sigma-Aldrich) and incubated for 30 min at room temperature. Again, cells were centrifuged and resuspended in FACS buffer (1 mM EDTA; 25 mM HEPES, pH 7.0; 1% BSA in PBS without Ca^{2+} and Mg^{2+}). Subsequently, cells were strained (strainer 40 μm). Transfected cells were sorted using a FACS Aria III cell sorter (BD Biosience; 488 nm argon laser) and thereafter recultivated as described. This process was repeated 2–3 times to increase enrichment of stably transfected cells.

Small interfering RNA (siRNA) silencing of gene expression

Chemically synthesized double-stranded siRNA duplexes (with 3′-dTdT overhangs) were obtained from Qiagen for the following targets: *GRK2* (5′-AAGAAAUUCAUUGAGAGCGAU-3′) and *GRK3* (5′-AAGCAAGCUGUAGAACACGUA-3′), and from GE Dharmacon a non-silencing RNA duplex (5′-GCUUAGGAGCAUUAGUAAA-3′ and 3′-UUUACUAAUGCUCCUAAGC-5′). Stably HA-hNOP receptor expressing HEK293 cells were transfected with 150 nM siRNA for single transfection or with 100 nM of each siRNA for double transfection for 3 days using HiPerFect. All experiments showed target protein abundance reduced by ≥80%.

Whole cell phosphorylation assays

Phosphorylation studies were carried out as described (123–125). Stable HA-hNOP receptor or 6S/TA expressing HEK293 cells were labeled with [^{32}P]orthophosphate (285 Ci/mg P_i; ICN, Eschwege) for 60 min at 37 °C. Labeled cells were incubated with 10 μM N/OFQ or vehicle for 10 min at 37 °C. Subsequently cells were placed on ice and scratched into precipitation buffer (50 mM Tris-HCl, pH 7.4; 150 mM NaCl; 5 mM EDTA; 10 mM NaF; 10 mM disodium pyrophosphate; 1% Nonidet P-40; 0.5% sodium deoxycholate; 0.1% SDS) in the presence of protease and phosphatase inhibitors cOmplete mini® and PhosSTOP® (Roche Diagnostics) and solubilized. HA-tagged hNOP receptors were immunoprecipitated using 50 μl anti-HA-agarose beads (ThermoFisher Scientific) and receptors were eluted in SDS-sample buffer for 30 min at 50 °C. Samples were size-separated on 7.5% SDS polyacrylamide gels followed by autoradiography.

Western blot analysis

Stably transfected cells were plated onto poly-L-lysine-coated 60-mm dishes and grown for 2 days to 80% confluency. After treatment with agonists or antagonists, cells were lysed with detergent buffer (50 mM Tris-HCl, pH 7.4; 150 mM NaCl; 5 mM EDTA; 10 mM NaF; 10 mM disodium pyrophosphate; 1% Nonidet P-40; 0.5% sodium deoxycholate; 0.1% SDS) in the presence of protease and phosphatase inhibitors. Where indicated, cells were preincubated with GRK2/3 inhibitor compound 101 or NOP receptor antagonists for 30 min before agonist exposure. After 30 min centrifugation at 4 °C, HA-tagged hNOP receptors were enriched using anti-HA-agarose beads. Samples were inverted for 1.5 hours at 4 °C.

Where indicated, samples were dephosphorylated with lambda protein phosphatase (Santa Cruz) for 1 hour at 30 °C. After washing, proteins were eluted using SDS sample buffer for 30 min at 50 °C. Proteins were separated on 7.5% or 12% SDS-polyacrylamide gels, and after electroblotting, membranes were incubated with 0.1 μg/ml antibodies to $pSer^{346}$ (5034), $pSer^{351}$ (4876) or $pThr^{362}/Ser^{363}$ (4874) overnight at 4 °C, followed by detection using enhanced chemiluminescence detection (ECL) of bound antibodies (Thermo Fisher Scientific). Blots were subsequently stripped and reprobed with the phosphorylation-independent antibody to NOPR (4871) or antibody to HA-tag (0631) to ensure equal loading of the gels.

In vivo phosphorylation studies

First, the distribution of NOP receptor in NOP-eGFP mouse brain and periphery was examined. Briefly, mice (n=3) were euthanized under deep anesthesia and organs (brains, spinal cord, dorsal root ganglia, lungs, heart, kidneys, adrenal glands) were collected, flash frozen on dry ice and stored at −80 °C until biochemical analysis. In a second set of experiments, the ability of different NOP receptor agonists to induce NOP receptor phosphorylation in vivo was investigated. Mice (n=3 per compound) were given i.p. injections of NOP receptor agonists MCOPPB (30 mg/kg), SCH221510 (30 mg/kg), NNC 63–0532 (30 mg/kg), AT-202 (30 mg/kg) or Ro64–6198 (30 mg/kg), or NOP receptor antagonist SB 612111 (30 mg/kg), or vehicle. Animals were sacrificed 30 min after treatment. Brains were immediately dissected out, frozen on dry ice and stored at −80 °C until biochemical analysis. A dose-response study for NOP receptor agonist AT-202 to induce NOP receptor phosphorylation was also performed using NOP-eGFP animals. Mice (n=3 per dose) were given i.p. injections of different doses of AT-202 (0, 0.3, 3, 10, 30 mg/kg). Samples were weighed, transferred into ice-cold detergent buffer (50 mM Tris-HCL, pH 7.4; 150 mM NaCl; 5 mM EDTA; 10 mM NaF; 10 mM disodium pyrophosphate; 1% Nonidet P-40; 0.5% sodium deoxycholate; 0.1% SDS; containing protease and phosphatase inhibitors) and homogenized using MINILYS workplace homogenizer (Peqlab). After 1 hour lysis at 4 °C, tissue homogenates were centrifuged at 16000 × g for 30 min at 4 °C. Supernatants were immunoprecipitated with anti-GFP antibody (Roche) bound to protein G-agarose beads or anti-GFP beads (NanoTag) for 1.5 hours at 4 °C. After protein determination using a Bradford Assay Kit (Thermo Fisher Scientific), proteins were eluted from the beads with SDS-sample buffer for 30 min at 50 °C. Proteins were separated on 7.5% SDS-polyacrylamide gels and after electroblotting membranes were incubated with antibodies to $pSer^{351}$ (4878), $pSer^{346}$ (5034) or $pThr^{362}/Ser^{363}$ (4874) at a concentration of 0.1 μg/ml, followed by ECL detection of bound antibodies. Blots were stripped and reprobed with the phosphorylation-independent antibody to NOPR (4871) or antibody to GFP (Synaptic Systems) to confirm equal loading of the gels.

Analysis of NOP receptor internalization

Stably transfected HA-tagged hNOP receptor cells or receptor mutant cells were plated onto poly-L-lysine-coated coverslips and grown overnight. Cells were incubated with rabbit anti-HA antibody (0631) in serum-free medium for 2 hours at 4 °C. After agonist or antagonist exposure for 60 min at room temperature, cells were fixed with 4% paraformaldehyde and 0.2% picric acid in phosphate buffer (pH 6.9) for 30 min at room temperature. Subsequently,

cells were washed several times with phosphate buffer (22.6 ml/L 1 M NaH_2PO_4•H_2O; 77.4 ml/L 1 M Na_2HPO_4•H_2O; 0.1 % Triton X-100, pH 7.4), permeabilized and then incubated with an Alexa488-coupled goat anti-rabbit antibody (Invitrogen). Cells were mounted and internalization was examined using a Zeiss LSM510 META laser scanning confocal microscope. For quantitative internalization assays, cells were plated onto 24-well plates and grown overnight. Cells were preincubated with anti-HA antibody (0631) for 2 hours at 4 °C and then exposed to agonists or antagonists for 60 min at 37 °C. Subsequently, cells were fixed for 45 min at room temperature, washed 3 times with PBS and incubated with a peroxidase-conjugated secondary antibody (Santa Cruz). After washing, ABTS substrate was added and optical density was measured at 405 nm using a FlexStation 3 microplate reader (Molecular Devices).

Primary culture of ventral midbrain neurons.

Ventral midbrain neurons were cultured using a procedure adapted from (126). The ventral mesencephalon was removed from embryonic day 14 (E14) NOPR-eYFP mice. Tissues were mechanically dissociated, incubated with 0.25% trypsin and 0.05% DNase in DPBS for 20 min at 37 °C, and triturated using ART 200 REACH Barrier pipette tips (ThermoFischer). Glass bottom dishes (Cellvis) were pre-coated overnight with 2 mg/ml poly-D-lysine, then rinsed three times with sterile water and dried prior to use on the day of dissections. Trituration and initial plating was performed in DMEM+ (DMEM/F12 with HEPES, supplemented with 10% fetal bovine serum, 1x B27 additive, 1 μg/ml glucose, and 1x penicillin-streptomyocin). Dissociated neurons were diluted to 1 million cells/ml in DMEM + and plated as a 50 μl drop in the center well of the glass bottom dishes. The dishes were incubated for 1 hour at 37 °C, 5% CO_2 to let the cells adhere, then 2ml of a 2:1 solution of DMEM+:NB+ was added to the dish (NB+: neurobasal medium supplemented with B27 additive, 1x penicillin/streptomycin, and L-glutamine). Every 2–3 days, one half of the medium was replaced with NB+.

NOP receptor internalization studies in primary ventral midbrain neurons.

Dissociated cultures of ventral midbrain neurons from NOPR-eYFP mice were imaged at DIV 7–10 using an Andor Revolution imaging system consisting of a Leica DMI6000B microscope, a Yokogawa CSU-X1 spinning-disk unit, an Andor iXon electron-multiplying charge-coupled device camera, and a laser combiner with four solid state lasers, all controlled using Andor iQ3 software. All imaging was performed inside a temperature-controlled chamber held at 37 °C, 5% CO_2. Images were acquired using a 63x oil immersion objective, 515 nm laser excitation, and 8 sec exposure time.

Membrane potential assay

Membrane potential was measured as previously described (94). Stably HA-hNOP receptor transfected AtT20 cells were plated into 96-well plates. Cells were washed with Hankś balanced salt solution (HBSS), buffered with 20 mM HEPES pH 7.4, containing 1.3 mM $CaCl_2$; 5.4 mM KCl; 0.4 mM K_2HPO_4; 0.5 mM $MgCl_2$; 0.4 mM $MgSO_4$; 136.9 mM NaCl; 0.3 mM Na_2HPO_4; 4.2 mM $NaHCO_3$; 5.5 mM glucose. Subsequently, cells were incubated with membrane potential dye (FLIPR Membrane Potential kit BLUE, Molecular Devices) for 45 min at 37 °C. Compounds and vehicle were injected in a final volume of 20 μl. The

initial volume in the wells was 180 μL (90 μL buffer plus 90 μL dye) and 20 μL of compound was added to the cells resulting in a final volume in the well of 200 μL and a 1:10 dilution of the compound. Hence, the compounds were prepared at 10x concentrations. A baseline reading is measured for 60 seconds before compounds or buffer were injected. Measurements were accomplished at 37 °C using a FlexStation 3 microplate reader (Molecular Devices). The data was first normalized to the baseline and then subtracted from the buffer-only trace for each corresponding data point.

NanoLC-MS/MS analysis

After i.p. administration of saline or AT-202 (30 mg/kg) and GFP immunoprecipitation from 3 brains per condition, immunoprecipitates were boiled in SDS sample buffer for 5 min at 100 °C. Subsequently, brain extracts were alkylated in 90 mM iodoacetamide for 30 min in the dark, separated by SDS-PAGE on 10% polyacrylamide gels followed by gel staining with colloidal Coomassie blue. At the molecular weight of NOP receptor a band was excised and subjected to in-gel tryptic digestion using modified porcine trypsin (Promega) at 20 ng/μl. The dried peptides were extracted and analyzed by on-line nanoLC using an Ultimate 3000 system (Dionex) coupled to an ETD-enabled LTQ Orbitrap Velos mass spectrometer (Thermo Fisher Scientific) as described (122, 127). The survey scan MS was performed in the Orbitrap on the 300–2000 *m/z* mass range with the resolution set to a value of 60.000 at *m/z* 400. The 20 most intense ions per survey scan were selected for subsequent CID/ETD fragmentation, and the resulting fragments were analyzed in the linear trap (LTQ). The settings for the data-dependent decision tree-based CID/ETD method were as follows: ETD was performed for all precursor ions with charge states > 5. The normalized collision energy was set to 35% for CID. The reaction time was set to 100 ms and supplemental activation was enabled for ETD. Triple technical replicates were performed in some conditions.

All raw mass spectrometry files were processed with MaxQuant (v 1.5.5.1) for database search with the Andromeda search engine. Data were searched against SwissProt database with taxonomy Mus musculus (16761 sequences) implemented with the mouse NOP receptor-eGFP sequence. Enzyme specificity was set to trypsin/P and a maximum of three missed cleavages were allowed. Carbamidomethylation of cysteine was set as fixed modification whereas oxidation of methionine and phosphorylation of serine, threonine and tyrosine were set as variable modifications. The precursor mass tolerance was set to 20 ppm for the first search and 10 ppm for the main Andromeda database search. The mass tolerance in MS/MS mode was set to 0.8 Da. The required minimum peptide length was seven amino acids, and minimum number of unique peptides was set to one. Andromeda results were validated by the target-decoy approach using a reverse database and the false discovery rates (FDR) at the peptide-spectrum matches (PSM), protein and site levels were set to 1%. Phosphosite localization was evaluated based on the Phosphosite Localization Scoring and Localization Probability algorithm of the Andromeda search engine.

Data Analysis

Protein bands detected on Western blots were quantified using ImageJ 1.47v software. Data were analyzed using GraphPad Prism 5 software. Densitometry of every protein band was carried out with Image J. We used the same area size to perform densitometry for every

protein band from the same experiment for every phosphorylation site as well as the total receptor. Accordingly, an equally sized, empty area from the blot/film was measured to subtract this value as background signal from every measuring point. Finally, phosphorylation signals were normalized to the total receptor (phosphorylation-independent antibody; NOPR). Controls (MOCK or SCR) were defined as 100% and phosphorylation of every target protein was calculated as percentage phosphorylation in comparison to the respective control. Statistical analysis was carried out with two-way ANOVA followed by Bonferroni correction. P values <0.05 were considered statistically significant.

To compare the ability of different agonists to induce NOP-YFP internalization in primary cultures of ventral midbrain neurons, fluorescent puncta formation was used as a proxy for receptor internalization. This allowed analysis to be performed on images containing several neurons with many of overlapping neurites. It also allowed automated analysis over large numbers of images without the need to manually select regions corresponding to the plasma membrane and cell interior. Puncta identification and counting was performed using Python code that was based on the original approach and Matlab code developed by Aguet *et al.* 2013 (128). In order to quantitatively compare the extent of puncta formation across different conditions, the number of puncta per image was normalized to the total NOP-YFP intensity. The plot shows this “puncta density” for each condition relative to N/OFQ.

Supplementary Material

Refer to Web version on PubMed Central for supplementary material.

Acknowledgements:

We thank Ulrike Schiemenz, Julia Karius and Heike Stadler for excellent technical assistance. We thank Dr. Odile Burlet-Schiltz for access to the Proteome Infrastructure of Toulouse and Dr. Catherine Mollereau for insightful discussions on MS analyses.

Funding:

This work was supported by Interdisziplinäres Zentrum für klinische Forschung (Juniorprojekt J61) to A.M., the Deutsche Forschungsgemeinschaft grants SFB/TR166-TPC5, SCHU924/10–3 and SCHU924/18–1 to S.S., and in part by the Région Occitanie, European funds (Fonds Européen de Développement Régional, FEDER), Toulouse Métropole, the French Ministry of Research with the Investissement dÁvenir Infrastrucutures Nationales en Biologie et Santé (ProFI, Proteomics French Infrastructure project, ANR-10-INBS-08) and NIH-NIDA by grant R21-DA034929 to M.R.B., by grant K01-DA042219 to P.R.O. and by grant DA023281 to L.T..

References and Notes

1. Bunzow JR et al., Molecular cloning and tissue distribution of a putative member of the rat opioid receptor gene family that is not a mu, delta or kappa opioid receptor type. FEBS letters 347, 284–288 (1994). [PubMed: 8034019]
2. Fukuda K et al., cDNA cloning and regional distribution of a novel member of the opioid receptor family. FEBS letters 343, 42–46 (1994). [PubMed: 8163014]
3. Mollereau C et al., ORL1, a novel member of the opioid receptor family. Cloning, functional expression and localization. FEBS letters 341, 33–38 (1994). [PubMed: 8137918]
4. Wang JB et al., cDNA cloning of an orphan opiate receptor gene family member and its splice variant. FEBS letters 348, 75–79 (1994). [PubMed: 8026588]
5. Meunier JC et al., Isolation and structure of the endogenous agonist of opioid receptor-like ORL1 receptor. Nature 377, 532–535 (1995). [PubMed: 7566152]

6. Reinscheid RK et al., Orphanin FQ: a neuropeptide that activates an opioidlike G protein-coupled receptor. Science 270, 792–794 (1995). [PubMed: 7481766]
7. Connor M, Yeo A, Henderson G, The effect of nociceptin on Ca2+ channel current and intracellular Ca2+ in the SH-SY5Y human neuroblastoma cell line. British journal of pharmacology 118, 205–207 (1996). [PubMed: 8735615]
8. Connor M, Christie MJ, Modulation of Ca2+ channel currents of acutely dissociated rat periaqueductal grey neurons. The Journal of physiology 509 (Pt 1), 47–58 (1998). [PubMed: 9547380]
9. Ikeda K. et al., Functional coupling of the nociceptin/orphanin FQ receptor with the G-protein-activated K+ (GIRK) channel. Brain research. Molecular brain research 45, 117–126 (1997). [PubMed: 9105677]
10. Beedle AM et al., Agonist-independent modulation of N-type calcium channels by ORL1 receptors. Nature neuroscience 7, 118–125 (2004). [PubMed: 14730309]
11. Yeon KY et al., Molecular mechanisms underlying calcium current modulation by nociceptin. Neuroreport 15, 2205–2209 (2004). [PubMed: 15371734]
12. Zhang NR et al., Serine 363 is required for nociceptin/orphanin FQ opioid receptor (NOPR) desensitization, internalization, and arrestin signaling. The Journal of biological chemistry 287, 42019–42030 (2012). [PubMed: 23086955]
13. Ruiz-Velasco V., Puhl HL, Fuller BC, Sumner AD, Modulation of Ca2+ channels by opioid receptor-like 1 receptors natively expressed in rat stellate ganglion neurons innervating cardiac muscle. The Journal of pharmacology and experimental therapeutics 314, 987–994 (2005). [PubMed: 15937148]
14. Knoflach F., Reinscheid RK, Civelli O., Kemp JA, Modulation of voltage-gated calcium channels by orphanin FQ in freshly dissociated hippocampal neurons. The Journal of neuroscience : the official journal of the Society for Neuroscience 16, 6657–6664 (1996). [PubMed: 8824306]
15. Lou LG, Ma L., Pei G., Nociceptin/orphanin FQ activates protein kinase C, and this effect is mediated through phospholipase C/Ca2+ pathway. Biochemical and biophysical research communications 240, 304–308 (1997). [PubMed: 9388473]
16. Lou LG, Zhang Z., Ma L., Pei G., Nociceptin/orphanin FQ activates mitogen-activated protein kinase in Chinese hamster ovary cells expressing opioid receptor-like receptor. Journal of neurochemistry 70, 1316–1322 (1998). [PubMed: 9489755]
17. Fukuda K. et al., Activation of phospholipase A2 by the nociceptin receptor expressed in Chinese hamster ovary cells. Journal of neurochemistry 71, 2186–2192 (1998). [PubMed: 9798946]
18. Fukuda K., Shoda T., Morikawa H., Kato S., Mori K., Activation of mitogen-activated protein kinase by the nociceptin receptor expressed in Chinese hamster ovary cells. FEBS letters 412, 290–294 (1997). [PubMed: 9256237]
19. Chan AS, Wong YH, Regulation of c-Jun N-terminal kinase by the ORL(1) receptor through multiple G proteins. The Journal of pharmacology and experimental therapeutics 295, 1094–1100 (2000). [PubMed: 11082445]
20. Zhang Z. et al., Endogenous delta-opioid and ORL1 receptors couple to phosphorylation and activation of p38 MAPK in NG108–15 cells and this is regulated by protein kinase A and protein kinase C. Journal of neurochemistry 73, 1502–1509 (1999). [PubMed: 10501195]
21. Chen Y. et al., Molecular cloning, tissue distribution and chromosomal localization of a novel member of the opioid receptor gene family. FEBS letters 347, 279–283 (1994). [PubMed: 8034018]
22. Narita M. et al., Identification of the G-protein-coupled ORL1 receptor in the mouse spinal cord by [35S]-GTPgammaS binding and immunohistochemistry. British journal of pharmacology 128, 1300–1306 (1999). [PubMed: 10578145]
23. Neal CR Jr. et al., Localization of orphanin FQ (nociceptin) peptide and messenger RNA in the central nervous system of the rat. The Journal of comparative neurology 406, 503–547 (1999). [PubMed: 10205026]
24. Neal CR Jr. et al., Opioid receptor-like (ORL1) receptor distribution in the rat central nervous system: comparison of ORL1 receptor mRNA expression with (125)I-[(14)Tyr]-orphanin FQ binding. The Journal of comparative neurology 412, 563–605 (1999). [PubMed: 10464356]

25. Florin S., Meunier J., Costentin J., Autoradiographic localization of [3H]nociceptin binding sites in the rat brain. Brain research 880, 11–16 (2000). [PubMed: 11032985]
26. Ozawa A. et al., Knock-In Mice with NOP-eGFP Receptors Identify Receptor Cellular and Regional Localization. The Journal of neuroscience : the official journal of the Society for Neuroscience 35, 11682–11693 (2015). [PubMed: 26290245]
27. Andero R., Nociceptin and the nociceptin receptor in learning and memory. Progress in neuro-psychopharmacology & biological psychiatry 62, 45–50 (2015). [PubMed: 25724763]
28. Sandin J., Georgieva J., Schott PA, Ogren SO, Terenius L., Nociceptin/orphanin FQ microinjected into hippocampus impairs spatial learning in rats. The European journal of neuroscience 9, 194–197 (1997). [PubMed: 9042583]
29. Jenck F. et al., Orphanin FQ acts as an anxiolytic to attenuate behavioral responses to stress. Proceedings of the National Academy of Sciences of the United States of America 94, 14854–14858 (1997). [PubMed: 9405703]
30. Pomonis JD, Billington CJ, Levine AS, Orphanin FQ, agonist of orphan opioid receptor ORL1, stimulates feeding in rats. Neuroreport 8, 369–371 (1996). [PubMed: 9051812]
31. Florin S., Suaudeau C., Meunier JC, Costentin J., Nociceptin stimulates locomotion and exploratory behaviour in mice. European journal of pharmacology 317, 9–13 (1996). [PubMed: 8982713]
32. Shah S., Page CP, Spina D., Nociceptin inhibits non-adrenergic non-cholinergic contraction in guinea-pig airway. British journal of pharmacology 125, 510–516 (1998). [PubMed: 9806334]
33. Fischer A., Forssmann WG, Undem BJ, Nociceptin-induced inhibition of tachykinergic neurotransmission in guinea pig bronchus. The Journal of pharmacology and experimental therapeutics 285, 902–907 (1998). [PubMed: 9580642]
34. Peluso J., Gaveriaux-Ruff C., Matthes HW, Filliol D., Kieffer BL, Orphanin FQ/nociceptin binds to functionally coupled ORL1 receptors on human immune cell lines and alters peripheral blood mononuclear cell proliferation. Brain research bulletin 54, 655–660 (2001). [PubMed: 11403992]
35. Gavioli EC, de Medeiros IU, Monteiro MC, Calo G., Romao PR, Nociceptin/orphanin FQ-NOP receptor system in inflammatory and immune-mediated diseases. Vitamins and hormones 97, 241–266 (2015). [PubMed: 25677775]
36. Kapusta DR, Sezen SF, Chang JK, Lippton H., Kenigs VA, Diuretic and antinatriuretic responses produced by the endogenous opioid-like peptide, nociceptin (orphanin FQ). Life sciences 60, PL15–21 (1997).
37. Doggrell SA, Cardiovascular and renal effects of nociceptin/orphanin FQ: a new mediator to target? Current opinion in investigational drugs (London, England : 2000) 8, 742–749 (2007).
38. Zadori ZS et al., Nocistatin and nociceptin given centrally induce opioid-mediated gastric mucosal protection. Peptides 29, 2257–2265 (2008). [PubMed: 18930088]
39. Morini G., De Caro G., Guerrini R., Massi M., Polidori C., Nociceptin/orphanin FQ prevents ethanol-induced gastric lesions in the rat. Regulatory peptides 124, 203–207 (2005). [PubMed: 15544860]
40. Pan Z., Hirakawa N., Fields HL, A cellular mechanism for the bidirectional pain-modulating actions of orphanin FQ/nociceptin. Neuron 26, 515–522 (2000). [PubMed: 10839369]
41. Morgan MM, Grisel JE, Robbins CS, Grandy DK, Antinociception mediated by the periaqueductal gray is attenuated by orphanin FQ. Neuroreport 8, 3431–3434 (1997). [PubMed: 9427301]
42. Zaveri NT, Nociceptin Opioid Receptor (NOP) as a Therapeutic Target: Progress in Translation from Preclinical Research to Clinical Utility. Journal of medicinal chemistry 59, 7011–7028 (2016). [PubMed: 26878436]
43. Ciccocioppo R., Angeletti S., Sanna PP, Weiss F., Massi M., Effect of nociceptin/orphanin FQ on the rewarding properties of morphine. European journal of pharmacology 404, 153–159 (2000). [PubMed: 10980274]
44. Ciccocioppo R. et al., Attenuation of ethanol self-administration and of conditioned reinstatement of alcohol-seeking behaviour by the antiopioid peptide nociceptin/orphanin FQ in alcohol-preferring rats. Psychopharmacology 172, 170–178 (2004). [PubMed: 14624331]

45. Kotlinska J., Wichmann J., Legowska A., Rolka K., Silberring J., Orphanin FQ/nociceptin but not Ro 65–6570 inhibits the expression of cocaine-induced conditioned place preference. Behavioural pharmacology 13, 229–235 (2002). [PubMed: 12122313]
46. Kotlinska J. et al., Nociceptin inhibits acquisition of amphetamine-induced place preference and sensitization to stereotypy in rats. European journal of pharmacology 474, 233–239 (2003). [PubMed: 12921868]
47. Zhao RJ et al., Orphanin FQ/nociceptin blocks methamphetamine place preference in rats. Neuroreport 14, 2383–2385 (2003). [PubMed: 14663196]
48. Sakoori K., Murphy NP, Central administration of nociceptin/orphanin FQ blocks the acquisition of conditioned place preference to morphine and cocaine, but not conditioned place aversion to naloxone in mice. Psychopharmacology 172, 129–136 (2004). [PubMed: 14624329]
49. Khroyan TV, Polgar WE, Jiang F., Zaveri NT, Toll L., Nociceptin/orphanin FQ receptor activation attenuates antinociception induced by mixed nociceptin/orphanin FQ/mu-opioid receptor agonists. The Journal of pharmacology and experimental therapeutics 331, 946–953 (2009). [PubMed: 19713488]
50. Khroyan TV et al., Differential effects of nociceptin/orphanin FQ (NOP) receptor agonists in acute versus chronic pain: studies with bifunctional NOP/mu receptor agonists in the sciatic nerve ligation chronic pain model in mice. The Journal of pharmacology and experimental therapeutics 339, 687–693 (2011). [PubMed: 21859931]
51. Khroyan TV et al., SR 16435 [1-(1-(bicyclo[3.3.1]nonan-9-yl)piperidin-4-yl)indolin-2-one], a novel mixed nociceptin/orphanin FQ/mu-opioid receptor partial agonist: analgesic and rewarding properties in mice. The Journal of pharmacology and experimental therapeutics 320, 934–943 (2007). [PubMed: 17132815]
52. Sukhtankar DD, Zaveri NT, Husbands SM, Ko MC, Effects of spinally administered bifunctional nociceptin/orphanin FQ peptide receptor/mu-opioid receptor ligands in mouse models of neuropathic and inflammatory pain. The Journal of pharmacology and experimental therapeutics 346, 11–22 (2013). [PubMed: 23652222]
53. Zaveri N., Peptide and nonpeptide ligands for the nociceptin/orphanin FQ receptor ORL1: research tools and potential therapeutic agents. Life sciences 73, 663–678 (2003). [PubMed: 12801588]
54. Toll L. et al., Comparison of the antinociceptive and antirewarding profiles of novel bifunctional nociceptin receptor/mu-opioid receptor ligands: implications for therapeutic applications. The Journal of pharmacology and experimental therapeutics 331, 954–964 (2009). [PubMed: 19773529]
55. Chang SD et al., Novel Synthesis and Pharmacological Characterization of NOP Receptor Agonist 8-[(1S,3aS)-2,3,3a,4,5,6-Hexahydro-1H-phenalen-1-yl]-1-phenyl-1,3,8-triazaspiro[4 .5]decan-4-one (Ro 64–6198). ACS chemical neuroscience 6, 1956–1964 (2015). [PubMed: 26367173]
56. Podlesnik CAet al., The effects of nociceptin/orphanin FQ receptor agonist Ro 64–6198 and diazepam on antinociception and remifentanil self-administration in rhesus monkeys. Psychopharmacology 213, 53–60 (2011). [PubMed: 20852848]
57. Reiss D., Wichmann J., Tekeshima H., Kieffer BL, Ouagazzal AM, Effects of nociceptin/orphanin FQ receptor (NOP) agonist, Ro64–6198, on reactivity to acute pain in mice: comparison to morphine. European journal of pharmacology 579, 141–148 (2008). [PubMed: 18031727]
58. Christoph A., Eerdekens MH, Kok M., Volkers G., Freynhagen R., Cebranopadol, a novel first-in-class analgesic drug candidate: first experience in patients with chronic low back pain in a randomized clinical trial. Pain 158, 1813–1824 (2017). [PubMed: 28644196]
59. Linz K. et al., Cebranopadol: a Novel Potent Analgesic Nociceptin/Orphanin FQ Peptide and Opioid Receptor Agonist. The Journal of pharmacology and experimental therapeutics, (2014).
60. Kleideiter E., Piana C., Wang S., Nemeth R., Gautrois M., Clinical Pharmacokinetic Characteristics of Cebranopadol, a Novel First-in-Class Analgesic. Clinical pharmacokinetics, (2017).
61. Tzschentke TM, Linz K., Frosch S., Christoph T., Antihyperalgesic, Antiallodynic, and Antinociceptive Effects of Cebranopadol, a Novel Potent Nociceptin/Orphanin FQ and Opioid Receptor Agonist, after Peripheral and Central Administration in Rodent Models of Neuropathic Pain. Pain practice : the official journal of World Institute of Pain, (2017).

62. Linz K. et al., Cebranopadol: a novel potent analgesic nociceptin/orphanin FQ peptide and opioid receptor agonist. The Journal of pharmacology and experimental therapeutics 349, 535–548 (2014). [PubMed: 24713140]
63. Rizzi A. et al., Pharmacological characterization of cebranopadol a novel analgesic acting as mixed nociceptin/orphanin FQ and opioid receptor agonist. Pharmacology research & perspectives 4, e00247 (2016).
64. Dahan A. et al., Respiratory Effects of the Nociceptin/Orphanin FQ Peptide and Opioid Receptor Agonist, Cebranopadol, in Healthy Human Volunteers. Anesthesiology 126, 697–707 (2017). [PubMed: 28291085]
65. Linz K., Schroder W., Frosch S., Christoph T., Opioid type Respiratory Depressant Side Effects of Cebranopadol in Rats Are Limited by Its Nociceptin/Orphanin FQ Peptide Receptor Agonist Activity. Anesthesiology 126, 708–715 (2017). [PubMed: 28291086]
66. Ding HK, Yasuda N., Daga D., Polgar PR, Lu WE, Czoty JJ, Kishioka PW, Zaveri S,NT, Ko MC, A bifunctional nociceptin and mu opioid receptor agonist is analgesic without opioid side effects in nonhuman primates. Sci.Transl.MEd 10, (2018).
67. Gunther T. et al., Targeting multiple opioid receptors - improved analgesics with reduced side effects? British journal of pharmacology, (2017).
68. Ranjan R., Pandey S., Shukla AK, Biased Opioid Receptor Ligands: Gain without Pain. Trends in endocrinology and metabolism: TEM 28, 247–249 (2017). [PubMed: 28110810]
69. Severino AL et al., Pain Therapy Guided by Purpose and Perspective in Light of the Opioid Epidemic. Frontiers in psychiatry 9, 119 (2018). [PubMed: 29740351]
70. Violin JD, Crombie AL, Soergel DG, Lark MW, Biased ligands at G-protein-coupled receptors: promise and progress. Trends in pharmacological sciences 35, 308–316 (2014). [PubMed: 24878326]
71. Fossler MJ et al., Oliceridine (TRV130), a Novel G Protein-Biased Ligand at the mu-Opioid Receptor, Demonstrates a Predictable Relationship Between Plasma Concentrations and Pain Relief. I: Development of a Pharmacokinetic/Pharmacodynamic Model. Journal of clinical pharmacology, (2018).
72. Singla N. et al., A randomized, Phase IIb study investigating oliceridine (TRV130), a novel micro-receptor G-protein pathway selective (mu-GPS) modulator, for the management of moderate to severe acute pain following abdominoplasty. Journal of pain research 10, 2413–2424 (2017). [PubMed: 29062240]
73. Viscusi ER et al., A randomized, phase 2 study investigating TRV130, a biased ligand of the mu-opioid receptor, for the intravenous treatment of acute pain. Pain 157, 264–272 (2016). [PubMed: 26683109]
74. Soergel DG et al., Biased agonism of the mu-opioid receptor by TRV130 increases analgesia and reduces on-target adverse effects versus morphine: A randomized, double-blind, placebo-controlled, crossover study in healthy volunteers. Pain 155, 1829–1835 (2014). [PubMed: 24954166]
75. Altarifi AA et al., Effects of acute and repeated treatment with the biased mu opioid receptor agonist TRV130 (oliceridine) on measures of antinociception, gastrointestinal function, and abuse liability in rodents. Journal of psychopharmacology (Oxford, England) 31, 730–739 (2017).
76. Mori T. et al., Usefulness for the combination of G-protein- and beta-arrestin-biased ligands of mu-opioid receptors: Prevention of antinociceptive tolerance. Molecular pain 13, 1744806917740030 (2017).
77. DeWire SM et al., A G protein-biased ligand at the mu-opioid receptor is potently analgesic with reduced gastrointestinal and respiratory dysfunction compared with morphine. The Journal of pharmacology and experimental therapeutics 344, 708–717 (2013). [PubMed: 23300227]
78. Chang SD et al., Quantitative Signaling and Structure-Activity Analyses Demonstrate Functional Selectivity at the Nociceptin/Orphanin FQ Opioid Receptor. Molecular pharmacology 88, 502–511 (2015). [PubMed: 26134494]
79. Ferrari F. et al., In vitro functional characterization of novel nociceptin/orphanin FQ receptor agonists in recombinant and native preparations. European journal of pharmacology 793, 1–13 (2016). [PubMed: 27780725]

80. Allouche S., Noble F., Marie N., Opioid receptor desensitization: mechanisms and its link to tolerance. Frontiers in pharmacology 5, 280 (2014). [PubMed: 25566076]
81. Mann A., Illing S., Miess E., Schulz S., Different mechanisms of homologous and heterologous mu-opioid receptor phosphorylation. British journal of pharmacology 172, 311–316 (2015). [PubMed: 24517854]
82. Liu-Chen LY, Agonist-induced regulation and trafficking of kappa opioid receptors. Life sciences 75, 511–536 (2004). [PubMed: 15158363]
83. Bruchas MR, Chavkin C., Kinase cascades and ligand-directed signaling at the kappa opioid receptor. Psychopharmacology 210, 137–147 (2010). [PubMed: 20401607]
84. Dang VC, Christie MJ, Mechanisms of rapid opioid receptor desensitization, resensitization and tolerance in brain neurons. British journal of pharmacology 165, 1704–1716 (2012). [PubMed: 21564086]
85. Williams JT et al., Regulation of mu-opioid receptors: desensitization, phosphorylation, internalization, and tolerance. Pharmacological reviews 65, 223–254 (2013). [PubMed: 23321159]
86. Gendron L., Cahill CM, von Zastrow M., Schiller PW, Pineyro G., Molecular Pharmacology of delta-Opioid Receptors. Pharmacological reviews 68, 631–700 (2016). [PubMed: 27343248]
87. Doll C. et al., Agonist-selective patterns of micro-opioid receptor phosphorylation revealed by phosphosite-specific antibodies. British journal of pharmacology 164, 298–307 (2011). [PubMed: 21449911]
88. Doll C. et al., Deciphering micro-opioid receptor phosphorylation and dephosphorylation in HEK293 cells. British journal of pharmacology 167, 1259–1270 (2012). [PubMed: 22725608]
89. Just S. et al., Differentiation of opioid drug effects by hierarchical multi-site phosphorylation. Molecular pharmacology 83, 633–639 (2013). [PubMed: 23239825]
90. Doll C. et al., in British journal of pharmacology. (2011), vol. 164, pp. 298–307. [PubMed: 21449911]
91. Mandyam CD, Thakker DR, Standifer KM, Mu-opioid-induced desensitization of opioid receptor-like 1 and mu-opioid receptors: differential intracellular signaling determines receptor sensitivity. The Journal of pharmacology and experimental therapeutics 306, 965–972 (2003). [PubMed: 12750434]
92. Mandyam CD, Thakker DR, Christensen JL, Standifer KM, Orphanin FQ/nociceptin-mediated desensitization of opioid receptor-like 1 receptor and mu opioid receptors involves protein kinase C: a molecular mechanism for heterologous cross-talk. The Journal of pharmacology and experimental therapeutics 302, 502–509 (2002). [PubMed: 12130708]
93. Thakker DR, Standifer KM, Induction of G protein-coupled receptor kinases 2 and 3 contributes to the cross-talk between mu and ORL1 receptors following prolonged agonist exposure. Neuropharmacology 43, 979–990 (2002). [PubMed: 12423667]
94. Gunther T., Culler M., Schulz S., Research Resource: Real-Time Analysis of Somatostatin and Dopamine Receptor Signaling in Pituitary Cells Using a Fluorescence-Based Membrane Potential Assay. Molecular endocrinology (Baltimore, Md.) 30, 479–490 (2016).
95. Kawamoto H. et al., Discovery of the first potent and selective small molecule opioid receptor-like (ORL1) antagonist: 1-[(3R,4R)-1-cyclooctylmethyl-3- hydroxymethyl-4-piperidyl]-3-ethyl-1, 3-dihydro-2H-benzimidazol-2-one (J-113397). Journal of medicinal chemistry 42, 5061–5063 (1999). [PubMed: 10602690]
96. Zaratin PF et al., Modification of nociception and morphine tolerance by the selective opiate receptor-like orphan receptor antagonist (−)-cis-1-methyl-7-[[4-(2,6-dichlorophenyl)piperidin-1-yl]methyl]-6,7,8,9-tetrahy dro-5H-benzocyclohepten-5-ol (SB-612111). The Journal of pharmacology and experimental therapeutics 308, 454–461 (2004). [PubMed: 14593080]
97. Cippitelli A. et al., A key role for the N/OFQ-NOP receptor system in modulating nicotine taking in a model of nicotine and alcohol co-administration. Scientific reports 6, 26594 (2016). [PubMed: 27199205]
98. Seibold A., January BG, Friedman J., Hipkin RW, Clark RB, Desensitization of beta2-adrenergic receptors with mutations of the proposed G protein-coupled receptor kinase phosphorylation sites. The Journal of biological chemistry 273, 7637–7642 (1998). [PubMed: 9516468]

99. Tran TM et al., Characterization of agonist stimulation of cAMP-dependent protein kinase and G protein-coupled receptor kinase phosphorylation of the beta2-adrenergic receptor using phosphoserine-specific antibodies. Molecular pharmacology 65, 196–206 (2004). [PubMed: 14722251]
100. Iyer V. et al., Differential phosphorylation and dephosphorylation of beta2-adrenoceptor sites Ser262 and Ser355,356. British journal of pharmacology 147, 249–259 (2006). [PubMed: 16331289]
101. Vaughan DJ et al., Role of the G protein-coupled receptor kinase site serine cluster in beta2-adrenergic receptor internalization, desensitization, and beta-arrestin translocation. The Journal of biological chemistry 281, 7684–7692 (2006). [PubMed: 16407241]
102. Fan X. et al., Cardiac beta2-Adrenergic Receptor Phosphorylation at Ser355/356 Regulates Receptor Internalization and Functional Resensitization. PloS one 11, e0161373 (2016).
103. Gluck L. et al., Loss of morphine reward and dependence in mice lacking G protein-coupled receptor kinase 5. Biological psychiatry 76, 767–774 (2014). [PubMed: 24629717]
104. Tang H., Guo DF, Porter JP, Wanaka Y., Inagami T., Role of cytoplasmic tail of the type 1A angiotensin II receptor in agonist- and phorbol ester-induced desensitization. Circulation research 82, 523–531 (1998). [PubMed: 9529156]
105. Kim J. et al., Functional antagonism of different G protein-coupled receptor kinases for beta-arrestin-mediated angiotensin II receptor signaling. Proceedings of the National Academy of Sciences of the United States of America 102, 1442–1447 (2005). [PubMed: 15671181]
106. Illing S., Mann A., Schulz S., Heterologous regulation of agonist-independent mu-opioid receptor phosphorylation by protein kinase C. British journal of pharmacology 171, 1330–1340 (2014). [PubMed: 24308893]
107. Kliewer A., Mann A., Petrich A., Poll F., Schulz S., A transplantable phosphorylation probe for direct assessment of G protein-coupled receptor activation. PloS one 7, e39458 (2012).
108. Lehmann A., Kliewer A., Gunther T., Nagel F., Schulz S., Identification of Phosphorylation Sites Regulating sst3 Somatostatin Receptor Trafficking. Molecular endocrinology (Baltimore, Md.) 30, 645–659 (2016).
109. Petrich A. et al., Phosphorylation of threonine 333 regulates trafficking of the human sst5 somatostatin receptor. Molecular endocrinology (Baltimore, Md.) 27, 671–682 (2013).
110. Poll F. et al., Pasireotide and octreotide stimulate distinct patterns of sst2A somatostatin receptor phosphorylation. Molecular endocrinology (Baltimore, Md.) 24, 436–446 (2010).
111. Ferrari F. et al., In vitro pharmacological characterization of a novel unbiased NOP receptor-selective nonpeptide agonist AT-403. Pharmacology research & perspectives 5, (2017).
112. Bloms-Funke P., Gillen C., Schuettler AJ, Wnendt S., Agonistic effects of the opioid buprenorphine on the nociceptin/OFQ receptor. Peptides 21, 1141–1146 (2000). [PubMed: 10998549]
113. Ciccocioppo R. et al., Buprenorphine reduces alcohol drinking through activation of the nociceptin/orphanin FQ-NOP receptor system. Biological psychiatry 61, 4–12 (2007). [PubMed: 16533497]
114. Cremeans CM, Gruley E., Kyle DJ, Ko MC, Roles of mu-opioid receptors and nociceptin/orphanin FQ peptide receptors in buprenorphine-induced physiological responses in primates. The Journal of pharmacology and experimental therapeutics 343, 72–81 (2012). [PubMed: 22743574]
115. Lutfy K. et al., Buprenorphine-induced antinociception is mediated by mu-opioid receptors and compromised by concomitant activation of opioid receptor-like receptors. The Journal of neuroscience : the official journal of the Society for Neuroscience 23, 10331–10337 (2003). [PubMed: 14614092]
116. Wnendt S., Kruger T., Janocha E., Hildebrandt D., Englberger W., Agonistic effect of buprenorphine in a nociceptin/OFQ receptor-triggered reporter gene assay. Molecular pharmacology 56, 334–338 (1999). [PubMed: 10419552]
117. Higgins GA et al., Influence of the selective ORL1 receptor agonist, Ro64–6198, on rodent neurological function. Neuropharmacology 41, 97–107 (2001). [PubMed: 11445190]

118. Sim LJ, Xiao R., Childers SR, Identification of opioid receptor-like (ORL1) peptide-stimulated [35S]GTP gamma S binding in rat brain. Neuroreport 7, 729–733 (1996). [PubMed: 8733732]
119. Sim-Selley LJ, Vogt LJ, Childers SR, Vogt BA, Distribution of ORL-1 receptor binding and receptor-activated G-proteins in rat forebrain and their experimental localization in anterior cingulate cortex. Neuropharmacology 45, 220–230 (2003). [PubMed: 12842128]
120. Berthele A. et al., [3H]-nociceptin ligand-binding and nociceptin opioid receptor mrna expression in the human brain. Neuroscience 121, 629–640 (2003). [PubMed: 14568023]
121. Anton B. et al., Immunohistochemical localization of ORL-1 in the central nervous system of the rat. The Journal of comparative neurology 368, 229–251 (1996). [PubMed: 8725304]
122. Mouledous L., Froment C., Burlet-Schiltz O., Schulz S., Mollereau C., Phosphoproteomic analysis of the mouse brain mu-opioid (MOP) receptor. FEBS letters 589, 2401–2408 (2015). [PubMed: 26226422]
123. Pfeiffer M. et al., Homo- and heterodimerization of somatostatin receptor subtypes. Inactivation of sst(3) receptor function by heterodimerization with sst(2A). The Journal of biological chemistry 276, 14027–14036 (2001). [PubMed: 11134004]
124. Pfeiffer M. et al., Heterodimerization of substance P and mu-opioid receptors regulates receptor trafficking and resensitization. The Journal of biological chemistry 278, 51630–51637 (2003). [PubMed: 14532289]
125. Koch T. et al., C-terminal splice variants of the mouse mu-opioid receptor differ in morphine-induced internalization and receptor resensitization. The Journal of biological chemistry 276, 31408–31414 (2001). [PubMed: 11359768]
126. Lotharius J., Dugan LL, O'Malley KL, Distinct mechanisms underlie neurotoxin-mediated cell death in cultured dopaminergic neurons. The Journal of neuroscience : the official journal of the Society for Neuroscience 19, 1284–1293 (1999). [PubMed: 9952406]
127. Mouledous L. et al., GRK2 protein-mediated transphosphorylation contributes to loss of function of mu-opioid receptors induced by neuropeptide FF (NPFF2) receptors. The Journal of biological chemistry 287, 12736–12749 (2012). [PubMed: 22375000]
128. Aguet F., Antonescu CN, Mettlen M., Schmid SL, Danuser G., Advances in analysis of low signal-to-noise images link dynamin and AP2 to the functions of an endocytic checkpoint. Developmental cell 26, 279–291 (2013). [PubMed: 23891661]
129. Vizcaino JA et al., 2016 update of the PRIDE database and its related tools. Nucleic acids research 44, 11033 (2016). [PubMed: 27683222]

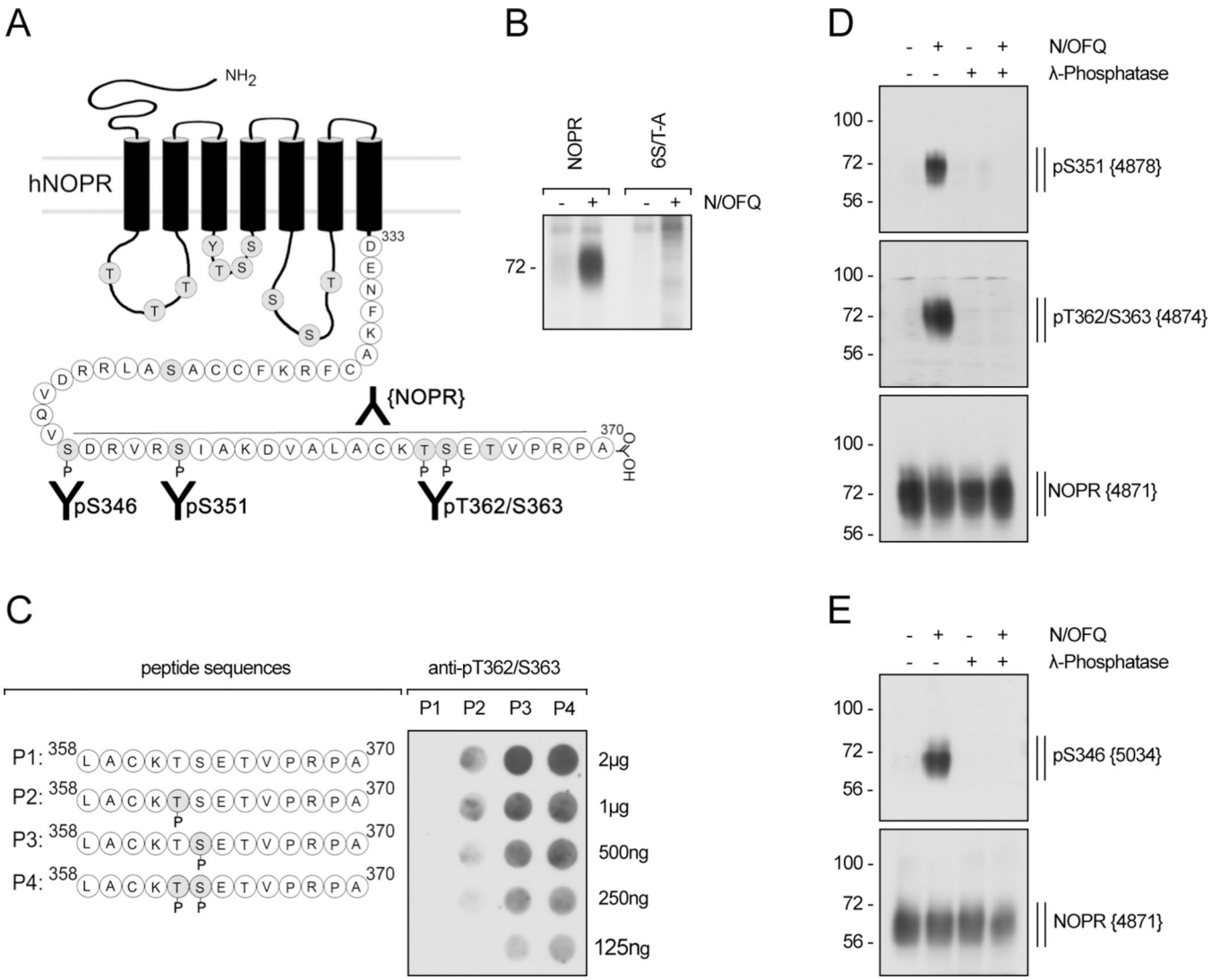

Figure 1: Characterization of phosphosite-specific NOP receptor antibodies.

(A) Schematic representation of the human nociceptin/orphanin FQ (hNOP) receptor. All potential intracellular phosphate acceptor sites are indicated (gray). Ser^{346}, Ser^{351} and Thr^{362}/Ser^{363} were targeted for the generation of phosphosite-specific antibodies and the epitope used for generating a phosphorylation-independent antibody (NOPR) is indicated by a black line. **(B)** HEK293 cells were transiently transfected with either the wild-type hNOP receptor or its 6S/T-A mutant. After 48 hours, cells were labeled with 200 µCi/ml carrier-free [^{32}P]orthophosphate. Labeled cells were either not treated (–) or treated (+) to 10 µM N/OFQ for 10 min, and whole-cell receptor phosphorylation was determined by SDS-polyacrylamide gel electrophoresis followed by autoradiography. **(C)** Dot-blot analysis on serial dilutions of peptides P1-P4 to characterize antibody to $pThr^{362}/pSer^{363}$. **(D and E)** Characterization of phosphosite-specific antibodies directed against Ser^{346}, Ser^{351} or Thr^{362}/Ser^{363} using λ-phosphatase. HEK293 cells stably expressing the HA-tagged hNOP receptor were either not treated (–) or treated (+) with 10 µM N/OFQ for 10 min. Lysates were then either incubated (+) or not (–) with λ-phosphatase and immunoblotted with the

phosphosite-specific antibodies to pSer^{346}, pSer^{351}, or pThr^{362}/Ser^{363}. Blots were stripped and reprobed with the phosphorylation-independent antibody to NOPR as a loading control. In all panels, blots are representative from one of three independent experiments. Molecular mass markers (kDA) are indicated, left.

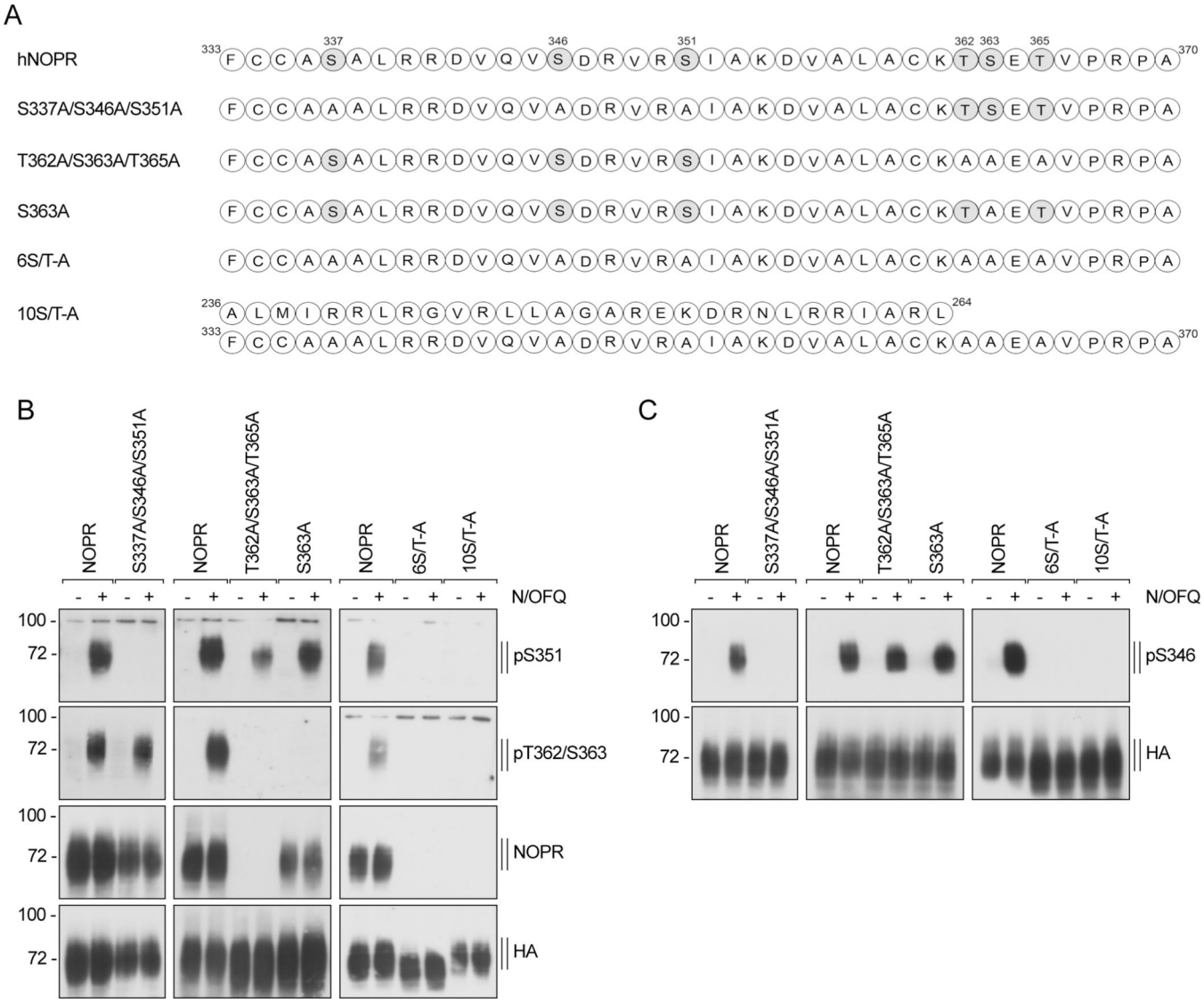

Figure 2: Characterization of phosphosite-specific NOP receptor antibodies using receptor mutants.

(A) Sequence of the carboxyl-terminal tail of the hNOP receptor showing all potential phosphate acceptor sites. Serine (S) and threonine (T) residues depicted in gray were exchanged to alanine. **(B and C)** HEK293 cells stably expressing HA-tagged hNOP, S337/346/351A, T362/S363/T365A, S363A, 6S/T-A, or NOP-10S/T-A were either not treated (–) or treated (+) with 10 μM N/OFQ for 10 min, and lysates were then immunoblotted with the antibodies to pSer^{346}, pSer^{351}, or pThr^{362}/Ser^{363}. Blots were stripped and reprobed with antibodies to NOPR or HA-tag. Blots are representative, (n=3).

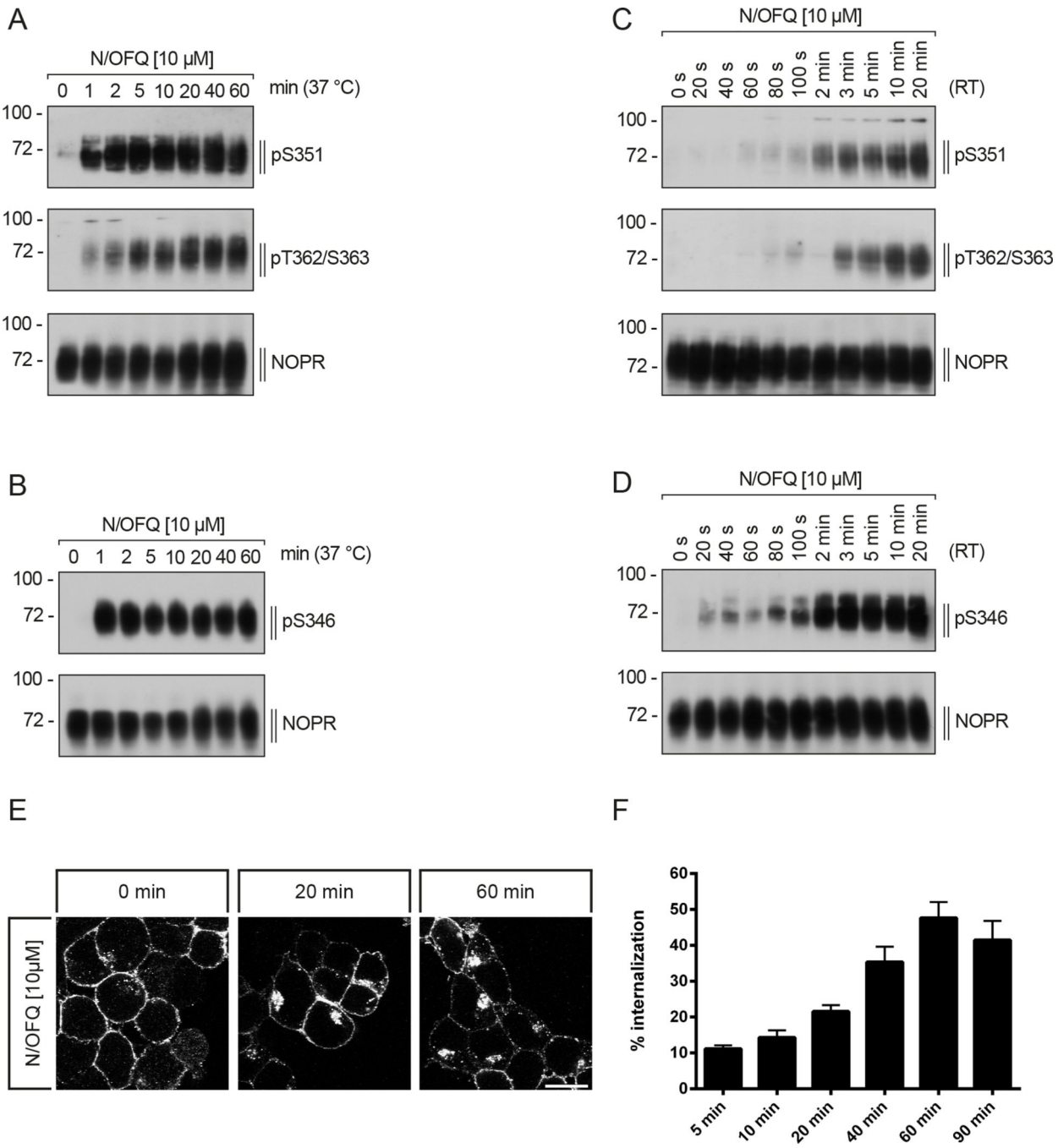

Figure 3: Time-course of N/OFQ-induced Ser^{346}, Ser^{351} and Thr^{362}/Ser^{363} phosphorylation and internalization.

(A to D) HEK293 cells stably expressing hNOP receptors were exposed to 10 μM N/OFQ for the indicated times and temperatures [(A and B) up to 60 min at 37 °C; (C and D) up to 20 min at 22 °C (room temperature, RT)], and lysates were immunoblotted with the indicated antibodies. Blots are representative of n=5 (A and C) or 6 (B and D) independent experiments. Blots were stripped and reprobed for NOPR. **(E)** HEK293 cells stably expressing the HA-tagged hNOP receptor were preincubated with antibody to HA-tag and

subsequently exposed to 10 μM N/OFQ for up to 60 min at 22 °C. Cells were fixed, permeabilized, immunofluorescently stained, and examined using confocal microscopy. Images are representative from one of three independent experiments. Scale bar, 20 μm. **(F)** Stably HA-tagged hNOP receptor-expressing HEK293 cells were preincubated with antibody to HA-tag and stimulated with 10 μM N/OFQ for up to 90 min at 37 °C. Cells were then fixed and labeled with a peroxidase-conjugated secondary antibody. Receptor internalization was measured by enzyme-linked immunosorbent assay and quantified as the percentage of internalized receptors in agonist-treated cells. Data are means ± SEM of six independent experiments performed in quadruplicate.

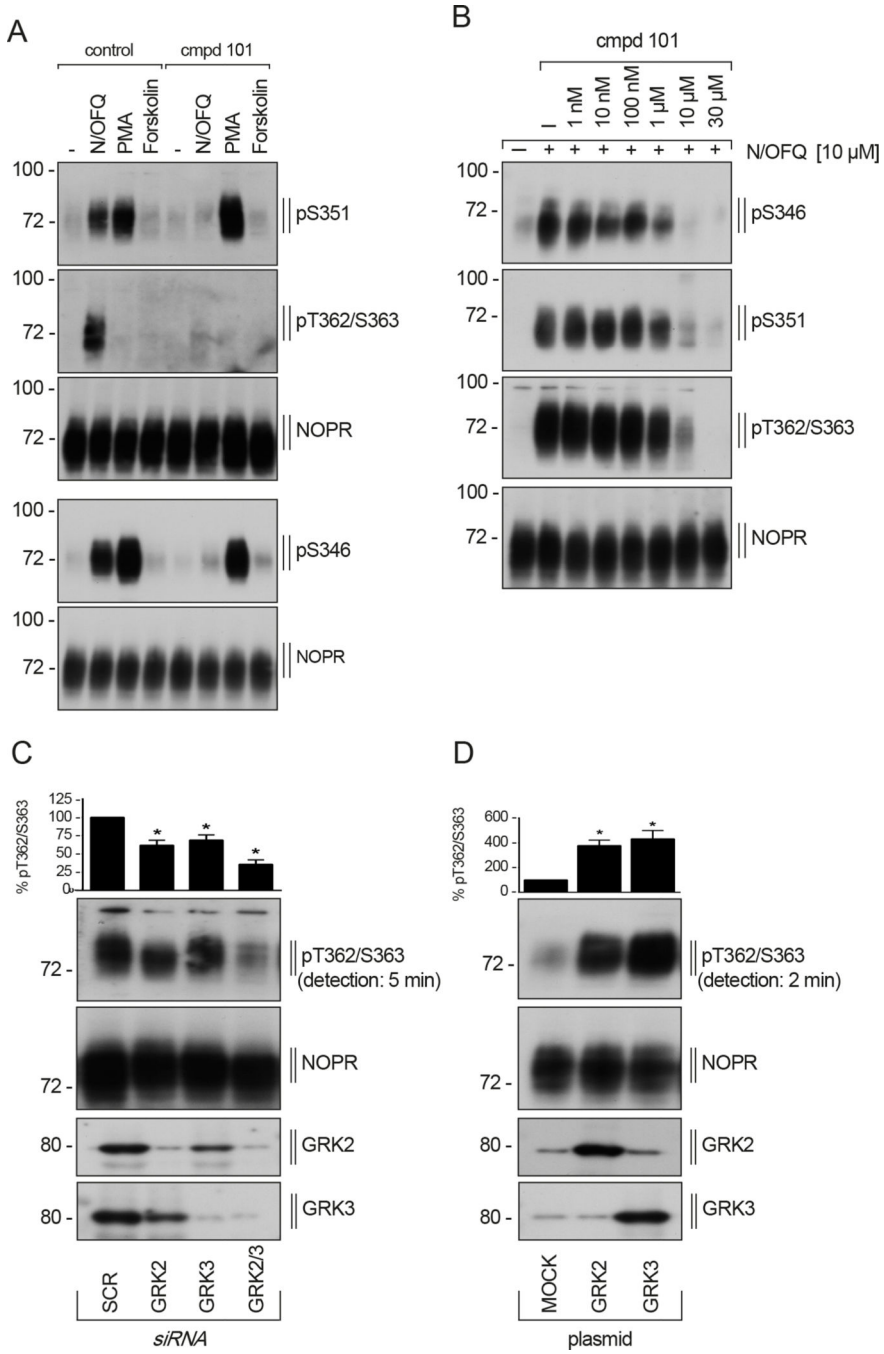

Figure 4: NOP receptor phosphorylation is mediated by GRK2 and GRK3.

(A) HEK293 cells stably expressing the hNOP receptor were preincubated with either vehicle (DMSO; control) or the GRK2/3-specific inhibitor compound 101 (cmpd 101) at 30 μM for 30 min at 37 °C, then exposed to 10 μM N/OFQ, 10 μM forskolin, or 1 μM PMA (or not, -) for 10 min. Lysates were then immunoblotted with antibodies to pSer^{346}, pSer^{351}, or pThr^{362}/Ser^{363}. Blots were stripped and reprobed for NOPR. Blots are representative, n=3. **(B)** Cells described in (A) were preincubated with vehicle (DMSO; (–) or cmpd101 at the indicated concentrations for 30 min at 37 °C, then treated with water (–) or 10 μM N/OFQ

for 10 min at 37 °C. Lysates were blotted as described in (A). Blots are representative, n=4. **(C and D)** Cells described in (A) were transfected with either siRNA targeting GRK2, GRK3, or GRK2 and GRK3 (GRK2/3) or a control (SCR) for 72 hours (C) or with GRK2 or GRK3 expression plasmids or an empty vector (MOCK) for 48 hours (D), then stimulated with 10 μM N/OFQ for 10 min at 37 °C. Lysates were immunoblotted with antibody to $pThr^{362}/Ser^{363}$. Blots were stripped and reprobed for NOPR. Densitometry, above the blots, was normalized to those in SCR- or MOCK-transfected cells, which were set to 100%. Data are mean ± SEM from five to six independent experiments. *$P<0.05$ vs. SCR or MOCK by two-way ANOVA with Bonferroni post-test.

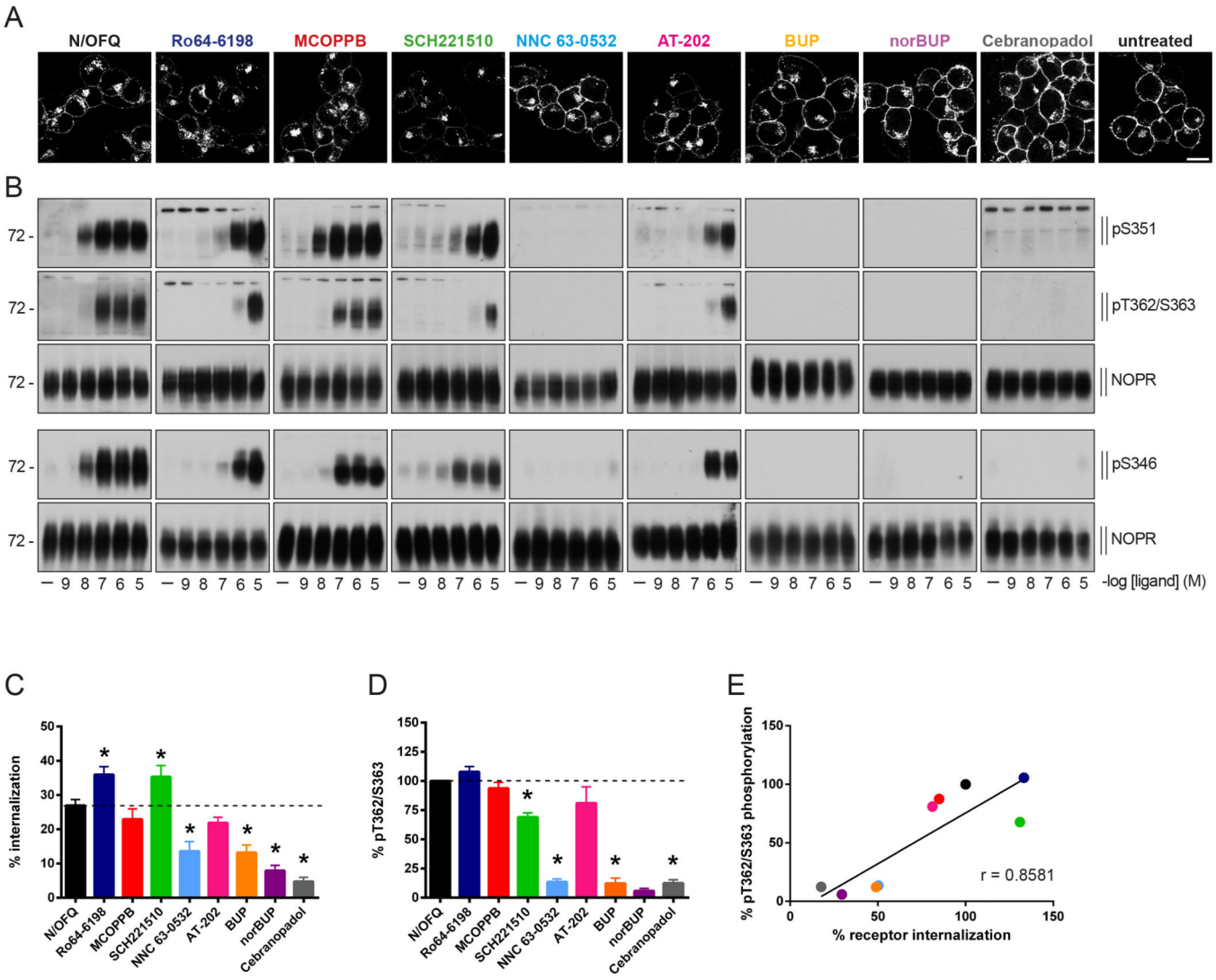

Figure 5: Agonist-selective NOP receptor phosphorylation and internalization.

(A) HEK293 cells stably expressing HA-tagged hNOP receptors were preincubated with HA antibody and then stimulated with 10 μM N/OFQ, Ro64–6198, MCOPPB, SCH221510, NNC 63–0532, AT-202, buprenorphine (BUP), norbuprenorphine (norBUP), cebranopadol or vehicle (according to the solvent) for 60 min at 22 °C. Cells were fixed, permeabilized, immunofluorescently stained, and subsequently examined using confocal microscopy. Images are representative, n=3 independent experiments. Scale bar, 20 μm. **(B)** NOP receptor-expressing HEK293 cells were treated with the compounds listed in (A) (–, vehicle solvent) at concentrations ranging from 10^{-9} to 10^{-5} M for 10 min at 37 °C, and lysates were immunoblotted with antibodies to pSer^{346}, pSer^{351}, or pThr^{362}/Ser^{363}. Blots were stripped and reprobed for NOPR. Blots are representative of n=3–5 experiments. **(C)** HEK293 cells stably expressing hNOP receptors were preincubated with antibody to HA-tag and treated with vehicle (solvent) or 10 μM N/OFQ, Ro64–6198, MCOPPB, SCH221510, NNC 63–0532, AT-202, BUP, norBUP or cebranopadol for 60 min at 37 °C. Cells were fixed and labeled with a peroxidase-conjugated secondary antibody. Receptor internalization was

measured by ELISA and quantified as the percentage of internalized receptors in agonist-treated cells. Data are means ± SEM from twelve independent experiments performed in quadruplicate. **(D)** Maximum NOP receptor ligand-induced phosphorylation at Thr^{362}/Ser^{363} from data in (B). Data are mean ± SEM from three independent experiments. *$P<0.05$ vs. N/OFQ by two-way ANOVA with Bonferroni post-test. **(E)** Correlation between NOP receptor phosphorylation and internalization induced by different ligands in HEK293 cells, from data in (A to D). Abscissae: ligand-induced internalization in percentage (normalized to N/OFQ). Ordinates: ligand-induced phosphorylation in percentage (normalized to N/OFQ). Solid line, linear regression of the data points; correlation coefficient r = 0.8581.

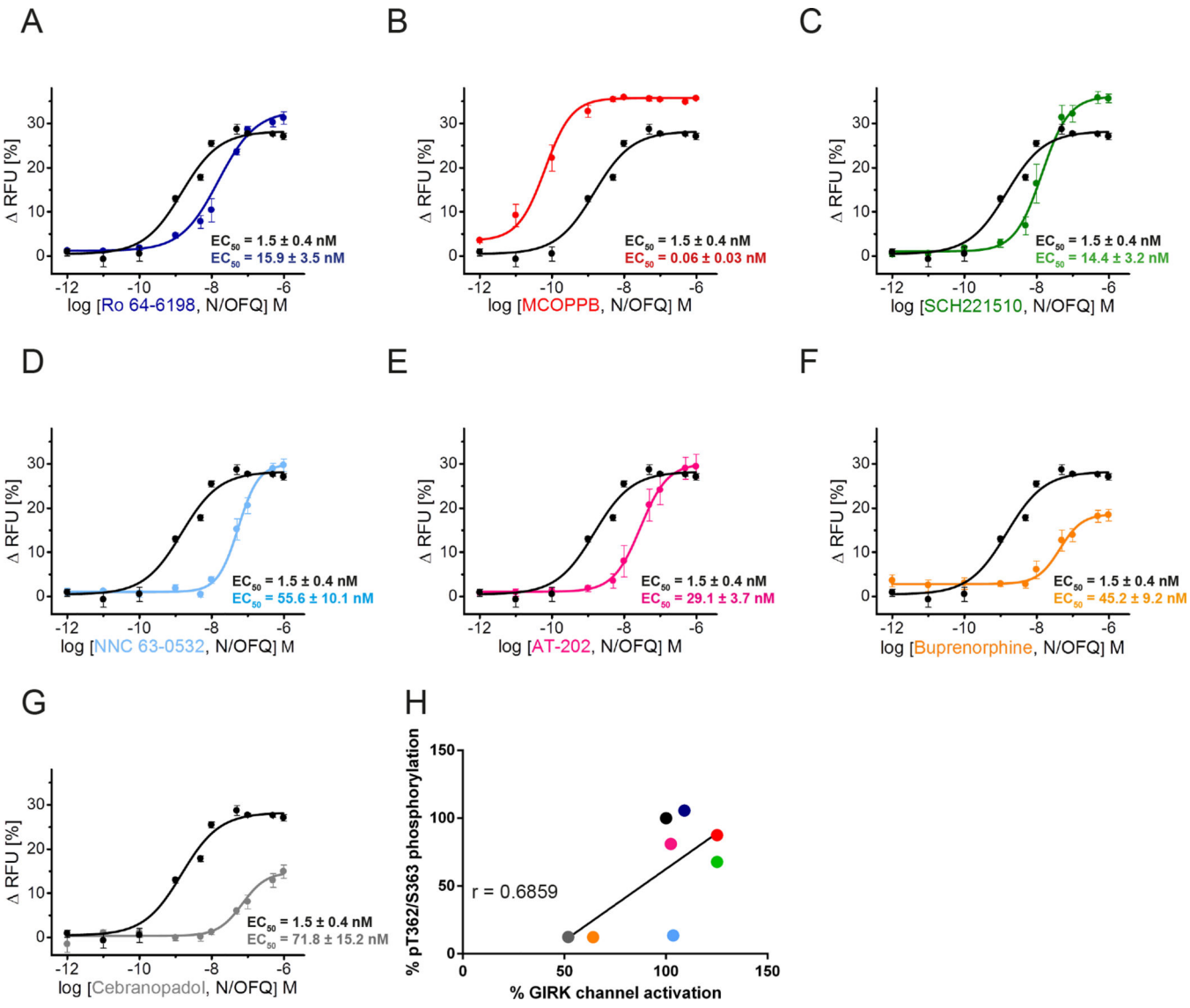

Figure 6: G protein signaling of chemically diverse NOP receptor agonists.

(A to G) Agonist-induced hyperpolarization can be measured by changes in fluorescence intensity of fluorescent oxonol dyes. A reduction of fluorescent signal intensity is indicative of Gβγ protein-mediated GIRK channel activation. AtT20 cells stably expressing the hNOP receptor were first preloaded with the dye. Thereafter, a baseline is measured for 60 seconds before cells were stimulated with vehicle (according to the solvent) or with Ro64–6198 (A), MCOPPB (B), SCH221510 (C), NNC 63–0532 (D), AT-202 (E), BUP (F), cebranopadol (G) or N/OFQ (A to G) at a concentration range of 10^{-6} to 10^{-13} M for 180 seconds. Dose-response curves were calculated with OriginPro using sigmoidal non-linear fitting. Vehicle-induced changes in fluorescence signal (background) were subtracted from signals obtained using agonist-containing solutions. Data are mean ± SEM from three independent experiments performed in duplicate. ΔRFU is change in relative fluorescence. **(H)** Correlation between NOP receptor phosphorylation (pThr^{362}/Ser^{363}) and GIRK channel activation induced by the different ligands, color-coordinated with (A to G). Abscissae:

ligand-induced G protein activation (EC_{50} values). Ordinates: ligand-induced phosphorylation in percentage (normalized to N/OFQ). Solid line, linear regression of the data points; correlation coefficient r = 0.6859.

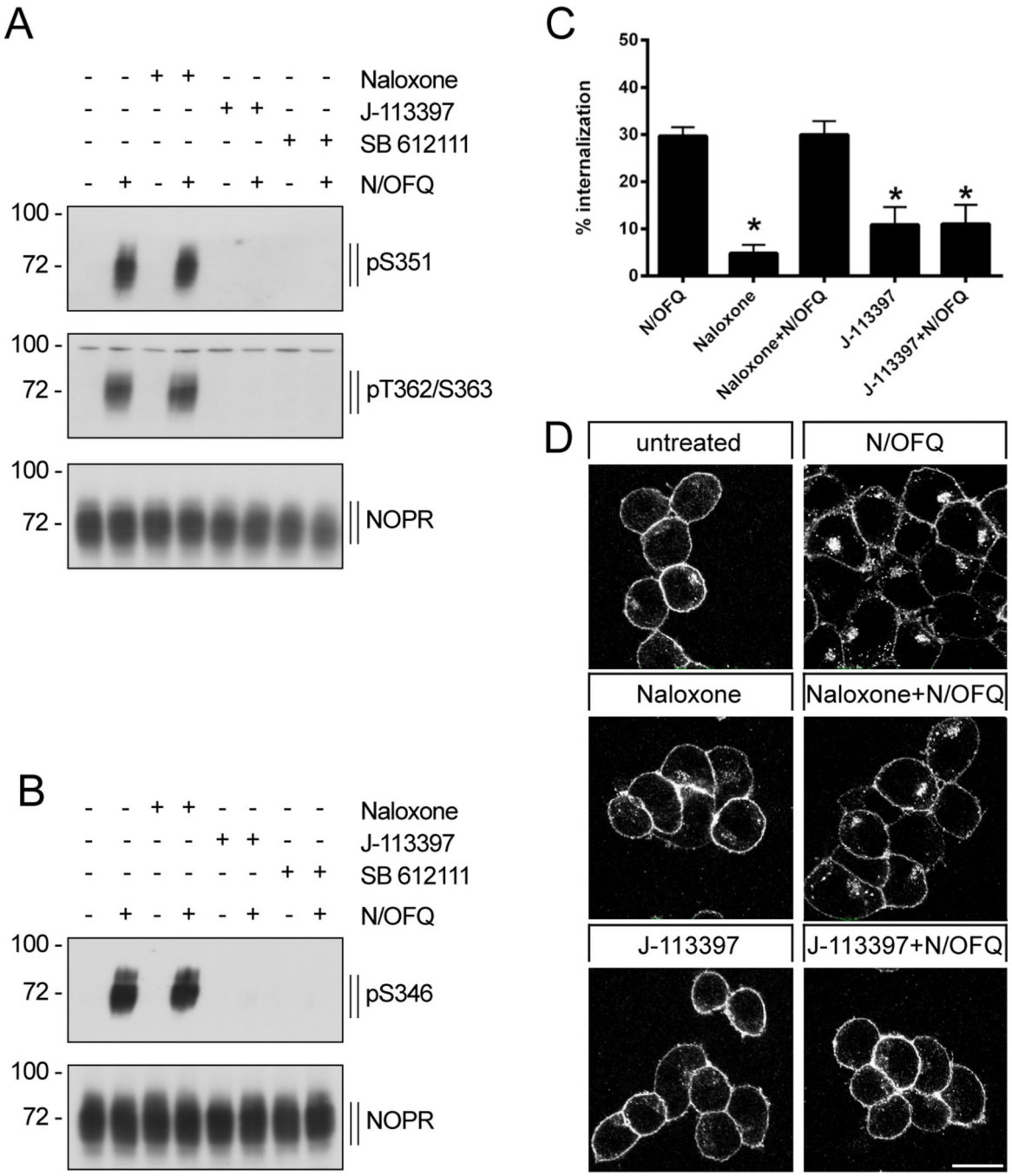

Figure 7: Antagonist-selective inhibition of N/OFQ-induced phosphorylation, internalization and G protein signaling.

(A and B) HEK293 cells stably expressing hNOP receptors were preincubated (+) or not (–) with 50 μM naloxone, J-113397, or SB 612111 for 30 min at 37 °C, then treated with vehicle (water; -) or with 10 μM N/OFQ (+) for 10 min at 37 °C. Cell lysates were then immunoblotted with antibodies to pSer^{346}, pSer^{351}, or pThr^{362}/Ser^{363}. Blots were stripped and reprobed for NOPR. Blots are representative, n=3. **(C)** HEK293 cells stably expressing the NOP receptor were preincubated with antibody to HA-tag and then treated with vehicle

(DMSO), 50 μM naloxone, J-113397, or SB 612111 and with or without 10 μM N/OFQ for 60 min at 37 °C. Cells were then fixed and labeled with a peroxidase-conjugated secondary antibody, and receptor internalization was measured by ELISA and quantified as percentage of internalized receptors in agonist-treated cells. Data are means ± SEM from six independent experiments performed in quadruplicate. *P<0.05 vs. N/OFQ by two-way ANOVA with Bonferroni post-test. **(D)** Cells described and treated as in (C), except treated at 22 °C, were fixed, permeabilized, immunofluorescently stained, and examined using confocal microscopy. Images are representative from one of three independent experiments. Scale bar, 20 μm.

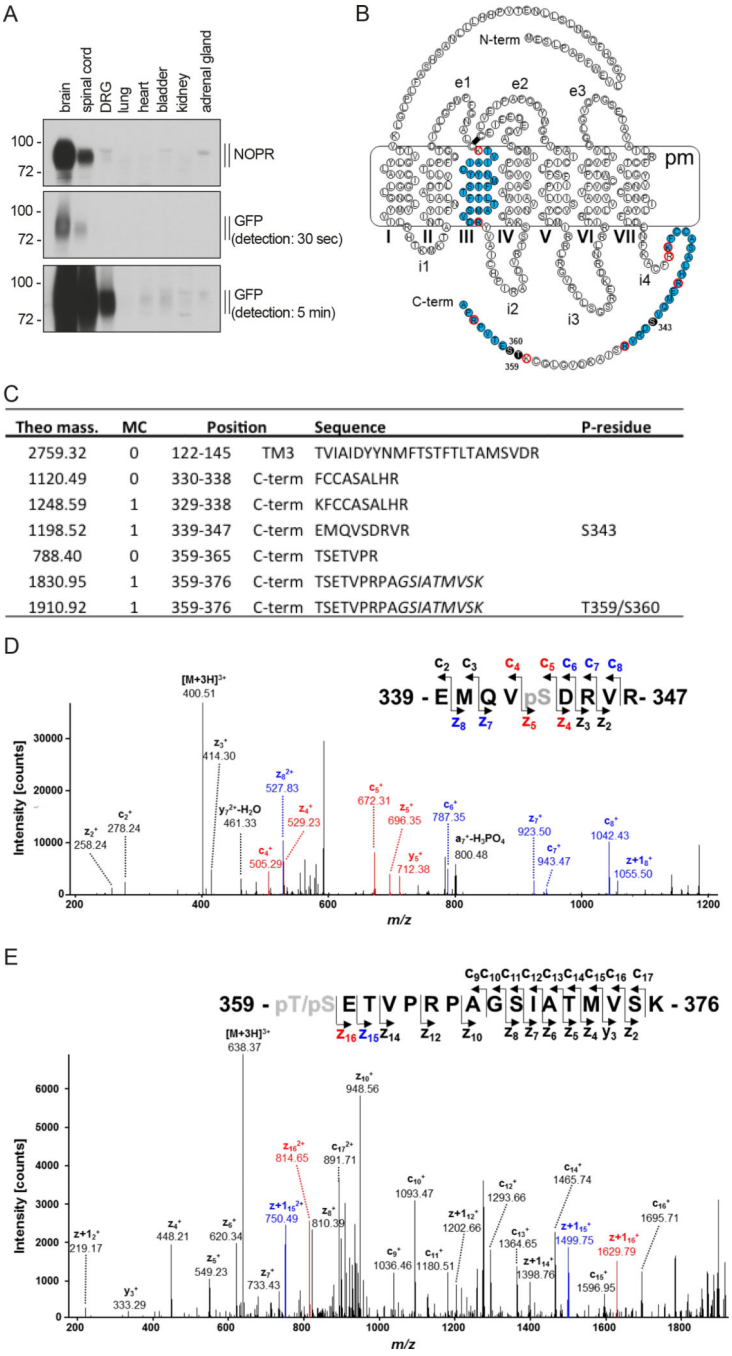

Figure 8: Tissue distribution of NOP receptor and NanoLC-MS/MS analysis of NOP receptor phosphorylation in vivo.

(A) Distribution of NOP receptor in NOP-eGFP knock-in mouse tissue. Anesthetized NOP-eGFP knock-in mice were sacrificed and tissues were removed. The NOP receptor was then immunoprecipitated from homogenates with anti-GFP protein agarose beads, and samples were immunoblotted with the phosphorylation-independent antibody to NOPR or antibody to GFP. Bottom, prolonged ECL detection exposure. Blots are representative from one of three independent experiments. **(B)** Mass spectrometry coverage of the NOP receptor sequence from mouse brain. The schema represents the secondary structure of the mouse

NOP receptor. Filled (blue and black) symbols indicate the protein sequence covered by nanoLC-MS/MS; the phosphorylated residues identified are black. Red circles indicate the trypsin cleavage sites. Pm, plasma membrane; e1-e3, extracellular loops; i1-i4, intracellular loops **(C)** List of phosphorylated and unphosphorylated NOP receptor peptides identified by nanoLC-MS/MS in the mouse brain. Amino acids belonging to the GFP sequence are in italics. Theo. Mass., theoretical mass (DA); MC, missed cleavage. **(D and E)** ETD MS/MS spectra of the monophosphorylated peptide 339-EMQVpSDRVR-347 (D; triply charged precursor ion, MH3+, at m/z 400.5128) and 359-pT/pSETVPRPAGSIATMVSK-376 (E; triply charged precursor ion, MH3+, at m/z 637.9797) display series of c- and z-ions indicating that Ser^{343} (D) and Thr^{359} or Ser^{360} (E) are phosphorylated, respectively. Red labels indicate site-determining ions and the corresponding peaks in the spectrum. Blue labels indicate fragment ions that confirm the site localization and exclude another potential site. pS, pT: phosphorylated serine or threonine residues.

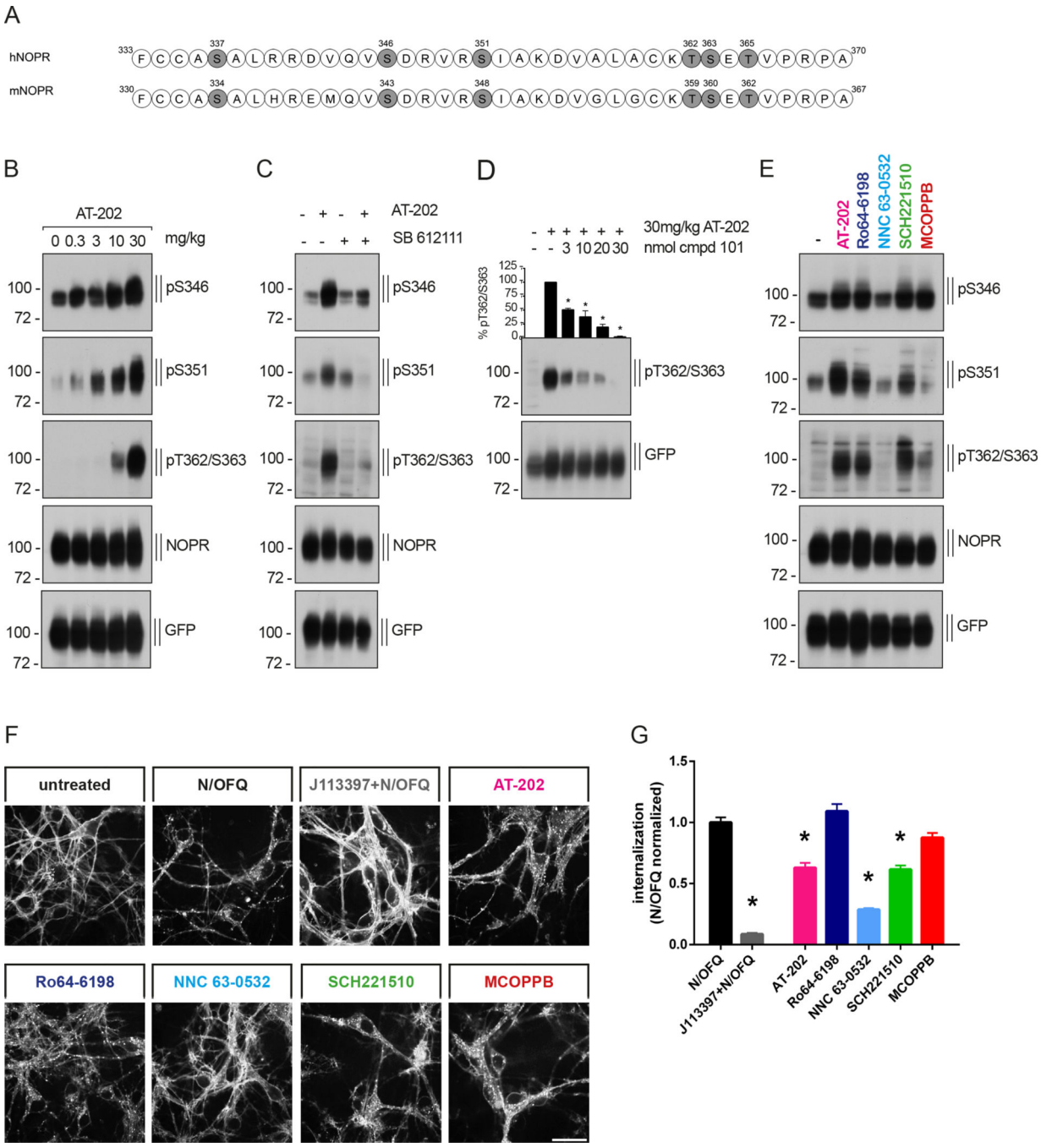

Figure 9: Agonist-selective NOP receptor phosphorylation in mouse brain.

(A) Schematic representation of the human (h) and mouse (m) nociceptin/orphanin FQ receptor. All potential intracellular phosphate acceptor sites are indicated (gray). **(B)** After i.p. injection of 0.9% NaCl (0) or AT-202 (0.3 to 30 mg/kg) for 30 min, NOP-eGFP knock-in mice were euthanized and brains were removed. NOP receptor was immunoprecipitated with anti-GFP protein agarose beads and immunoblotted with antibodies to pSer^{346}, pSer^{351}, or pThr^{362}/Ser^{363}. Blots were stripped and reprobed for NOPR or GFP. Blots are representative, n=3. **(C)** As in (B), but mice were treated with SB 612111 or AT-202 singly

or pretreated with SB 612111 for 30 min followed by AT-202 (each 30 mg/kg). **(D)** After intracerebroventricular injection of compound 101 (0.3 to 30 nmol), NOP-eGFP knock-in mice were treated with AT-202 (30 mg/kg for 30 min), euthanized and brains were removed. Homogenates underwent immunoprecipitation with anti-GFP agarose beads, and the resulting samples were immunoblotted for phosphorylated ($pThr^{362}/Ser^{363}$) NOP receptor. Blots were stripped and reprobed with the GFP antibody as a loading control. Blots are representative, n=3. **(E)** As in (B), but mice were treated with 0.9% NaCl (–) or 30 mg/kg AT-202, Ro64–6198, NNC 63–0532, SCH221510 or MCOPPB for 30 min. **(F and G)** Imaging (F) and analysis (G) of NOP receptor internalization in ventral midbrain neurons. Primary cultures from NOPR-eYFP mice were treated for 1 hour with 1 μM of the indicated agonist, followed by live cell spinning disk confocal imaging. Images are representative, and data are means ± SEM of over 40 images from at least two dishes per condition.

Table 1:

NOP receptor peptide sequences used for generation of phosphosite-specific antisera.

List of peptide sequences used for generating phosphosite-specific antibodies against individual phosphorylated forms of the NOP receptor and a phosphorylation-independent antiserum targeting the NOP receptor at the end of the carboxyl-terminal domain. Endogenous cysteine were exchanged (abu).

Antiserum Name	Sequence used for immunization	Amino acid position in human NOP receptor
Ser^{346}	REMQV-(p)S-DRVR	341–350
Ser^{351}	DRVR-(p)S-IAKDV	347–356
Thr^{362}/Ser^{363}	LG-abu-K-(p)T- (p)S-ETVPR	358–368
NOPR (phosphorylation-independent)	VRSIAKDVGLG-abu-KTSETVPRPA	349–370